Cancer Nanotechnology

RESEARCH

Open Access

Cabazitaxel-loaded human serum albumin nanoparticles combined with TGFβ-1 siRNA lipid nanoparticles for the treatment of paclitaxel-resistant non-small cell lung cancer

Tiantian Tan[1,2,3], Yuxin Feng[1,2,3], Weimin Wang[1,2,3], Rongrong Wang[1,2,3], Liyan Yin[2,3,4], Yiying Zeng[1,2,3], Zhaowu Zeng[1,2,3*] and Tian Xie[1,2,3*]

*Correspondence:
artgreenking@126.com;
xbs@hznu.edu.cn

[1] School of Pharmacy, Hangzhou Normal University, Hangzhou 311121, Zhejiang, People's Republic of China
[2] Key Laboratory of Elemene Class Anti-Cancer Chinese Medicine of Zhejiang Province, Hangzhou 311121, Zhejiang, People's Republic of China
[3] Engineering Laboratory of Development and Application of Traditional Chinese Medicine from Zhejiang Province, Hangzhou 311121, Zhejiang, People's Republic of China
[4] Traditional Chinese Medicine College of Guangdong Pharmaceutical University, Guangzhou 511400, People's Republic of China

Abstract

Background: In the current treatment of non-small cell lung cancer (NSCLC), traditional chemotherapy causes high toxicity, so it is necessary to develop safe chemical drug delivery vehicles clinically. Chemotherapy monotherapy is prone to drug resistance. Chemotherapy combined with other therapies such as nucleic acid drugs is an effective way to avoid drug resistance and the toxicity of continuous chemotherapy. In this study, chemotherapy and siRNA therapy were combined to treat paclitaxel-resistant NSCLC in order to increase efficacy and reduce toxicity. This study aims to develop a cabazitaxel-loaded human serum albumin nanoparticles (CTX-HSA-NPs) to improve the toxicity of traditional CTX-Tween 80 and increase targeting, and to develop a TGFβ-1 siRNA lipid Nanoparticles (TGFβ-1 siRNA LNP) combined with chemotherapy in the treatment of paclitaxel-resistant NSCLC.

Results: This study prepared CTX-HSA-NPs and TGFβ-1 siRNA LNP had small particle size, high encapsulation efficiency (EE). CTX-HSA-NPs lyophilized powder has high stability after dissolved. The antitumor effect of CTX-HSA-NPs on paclitaxel-resistant NSCLC was higher than that of CTX-Tween, and the toxicity was 1.8 times lower than that of CTX-Tween. More importantly, the combined treatment of TGFβ-1 siRNA LNP and CTX-HSA-NPs could effectively improve the antitumor efficacy of paclitaxel-resistant NSCLC in vivo and in vitro. The results of tumor immunohistochemistry showed that TGFβ-1 siRNA LNP significantly inhibited the expression of TGFβ-1, and compared with other groups, the expression of P-gp after low-dose CTX-HSA-NPs treatment was lower, which did not cause obvious drug resistance.

Conclusions: The antitumor effect of CTX-HSA-NPs on paclitaxel-resistant NSCLC was higher than that of CTX-Tween, and the toxicity was lower than that of CTX-Tween. TGFβ-1 siRNA LNP can treat paclitaxel-resistant NSCLC by inhibiting the express of *TGFβ-1* mRNA. The combined treatment of TGFβ-1 siRNA LNP and CTX-HSA-NPs could effectively improve the antitumor efficacy of paclitaxel-resistant NSCLC. A combination therapy of chemotherapy and nucleic acid drugs could be an effective approach for treating paclitaxel-resistant NSCLC.

Keywords: Cabazitaxel, Albumin, Paclitaxel-resistant NSCLC, Lipid nanoparticles, TGFβ-1 siRNA

Introduction

Lung cancer is currently the second most prevalent and the leading cause of cancer-related deaths worldwide (Sung et al. 2021). Chemotherapy is the common treatment for lung cancer globally. The current main treatments for lung cancer include standard chemotherapy (c paclitaxel, docetaxel), gene-targeted therapy for non-small cell lung cancer (erlotinib, afatinib, and gefitinib), and immune Checkpoint PD-L1/2 and PD-1 inhibitors (pembrolizumab, nivolumab, and atezolizumab), etc. (Reck et al. 2022). Currently, multidrug resistance (MDR) caused by the long-term use of standard chemotherapy has become a common problem (Król et al. 2010). The multidrug resistance mechanisms are diverse and complex, and statistics indicate that more than 90% of cancer deaths can be attributed to drug resistance (Mansoori et al. 2017). The development of drugs to treat or reverse drug resistance has become a focal point in the current research on drug-resistant tumors (Awasthi et al. 2018).

In the twenty-first century, nucleic acids are attracting attention as the next-generation modality beyond small molecules and antibodies. Small interfering RNA is a class of double-stranded non-coding RNA molecules of about 19–25 base pairs. RNA interference is a new way of treating cancer that uses small interfering RNA (siRNA) to silence gene expression (Mainini and Eccles 2020). This is achieved by siRNA binding to the target mRNA, which induces the degradation of the corresponding mRNA through the RNA-mediated silencing complex. siRNA-mediated gene silencing technology has wide application potential due to its high efficiency and specificity in degrading the integrity of target protein mRNA and inhibiting the expression of disease-related genes. siRNA drugs have numerous advantages, such as high efficiency, strong specificity, and easy assessment of therapeutic effects (Awasthi et al. 2018). In 2001, Elbashir et al. showed that synthetic siRNA restricts the specific arrangement of genes, and this property can be applied to treat diseases (Elbashir et al. 2001). In 2004, the first siRNA drug for treating wet age-related macular degeneration entered Phase I clinical trial (Whelan 2005). In 2010, the first targeted nanoparticle delivery system for patients with solid tumors entered phase I clinical trials, marking the start of the systemic application of siRNA in treating solid tumors (Whelan 2005). In August 2018, the FDA-approved ONPATTRO™ (Patisiran), the first siRNA therapy for treating transthyretin-mediated amyloidosis (Setten et al. 2019). Since the approval of "fomivirsen" in 1998, the first nucleic acid drug in the world, a total of 16 nucleic acid medicines, nine antisense oligonucleotides, four siRNA, one aptamer, and two messenger RNAs have been approved in certain regions in the United States, European Union, and Japan, as of May 2021 (Suzuki and Ishihara 2021).

Selecting specific multidrug-resistance targets is the most direct and effective way to treat multidrug-resistant lung cancer. Transforming growth factor beta-1 (TGFβ-1) has been linked to the occurrence and development of tumors and participates in mediating multidrug resistance in small-cell lung cancer (Liu et al. 2017). According to Kim et al. (2014) TGFβ-1 can induce epithelial–mesenchymal transition (EMT) and promote the migration, invasion, and anti-apoptosis of lung adenocarcinoma cells. Irigogen et al.

found a strong and positive correlation between the expression of TGFβ-1 and the sensitivity to cisplatin, paclitaxel, gemcitabine, and VP-16 by NSCLC (Irigoyen et al. 2010). The above studies demonstrate that silencing TGFβ-1 with siRNA could potentially be used for treating multidrug-resistant lung cancer. Therefore, in this study, we evaluated the prospect of targeting TGFβ-1 using TGFβ-1 siRNA for treating drug-resistant lung cancer. However, the efficient delivery of siRNA as a drug to tumors and the efficient silencing of target genes remains challenging. In vivo, siRNA drugs must overcome the vascular barrier to achieve endocytosis and lysosomal escape and avoid degradation by nucleases (Jackson and Linsley 2010). Naked siRNAs have difficulties entering cells. Selecting suitable carriers and delivery methods is necessary to mediate the smooth entry of siRNA into cells to exert its effect. The preparation of siRNAs into nanoparticles has the potential to overcome intravascular degradation and ensure the safe and efficient delivery of these molecules. Thus, this would enhance the accumulation of drugs at tumor sites through passive or active targeting (Guo et al. 2019). Currently, lipid nanoparticles (LNP) drug delivery systems are widely used. The first RNA interference drug was delivered into cells safely and effectively using a lipid nanoparticle delivery system. LNP is one of the most advanced nucleic acid delivery platforms with better biocompatibility and biodegradability, which can solve the delivery difficulties of nucleic acid drugs. Several studies have utilized lipid nanoparticles, such as PLGA–lipid hybrid nanoparticles synthesized using the emulsion method for siRNA delivery. The nanoparticles showed high encapsulation efficiency (up to 90%), and the delivered siRNA effectively downregulated the expression of the target gene in vitro and in vivo. Therefore, lipid nanoparticles are suitable systems for siRNA delivery.

In addition, chemotherapy drugs usually have poor solubility. Thus, abundant solubilizers must be added to improve their dissolution and absorption. In addition, they are highly toxic. Although the toxicity of chemotherapeutic drugs is unavoidable, it can be reduced by improving the formulation and can also be prepared into nanoparticles to improve their targeting efficiency. Nanoparticles decrease the toxicity to normal tissues and organs, ensuring effective chemotherapeutic antitumor effects but low toxicity. In addition, refractory drug-resistant tumors can be treated using a combination of traditional chemotherapy and siRNA drugs that inhibit multiple targets that would have required multiple drugs.

Taxanes are a class of small-molecule chemotherapeutic drugs that bind to the β-subunit of tubulin to inhibit the depolymerization of microtubules during mitosis, promoting the apoptosis of cancer cells (Arnst 2020). Currently, FDA-approved taxanes for clinical treatment include paclitaxel, docetaxel (Zhang et al. 2019), and cabazitaxel (CTX). Paclitaxel and docetaxel are first-generation taxanes used to treat various cancers, including ovarian, lung, and breast cancer, whereas cabazitaxel is a second-generation taxane for treating cancers. The semi-synthetic taxane formed by methyl etherification of 7,10-OH of docetaxel was developed to overcome taxane resistance (Muggia and Kudlowitz 2014). Taxane-sensitive cell lines revealed that the antiproliferative activity of cabazitaxel is comparable to that of docetaxel. Moreover, cabazitaxel has significantly higher activity in taxane-resistant cell lines (Vrignaud et al. 2014). Studies have shown that cabazitaxel is more effective than docetaxel in treating tumors resistant to taxane or with innate or acquired resistance (Vrignaud et al. 2013). Cabazitaxel

has a low affinity for P-gp and is appropriate for treating P-gp-mediated drug resistance (Duran et al. 2018). CTX-Tween was approved by the FDA in 2010, and is used clinically in combination with prednisone to treat hormone-refractory metastatic prostate cancer in patients who had previously received docetaxel (Malhotra et al. 2013). However, CTX-Tween also has several disadvantages, including high toxicity, poor safety, and poor water solubility, all common in chemotherapeutic drugs. Therefore, there is a need for a safe delivery vehicle for loading cabazitaxel to improve the safety of the formulations and enhance specificity.

In cancer therapy, nanoparticles have become drug delivery vehicles because they can be loaded with chemotherapeutic drugs and have a high target specificity (Awasthi et al. 2018). Compared to traditional formulations, nanopreparations can efficiently deliver drugs to target cells and ensure efficient cell uptake. Efficient delivery helps avoid unwanted effects on healthy cells and reduces adverse toxicity to patients. Drug resistance has a wide range of applications in drug delivery (Awasthi et al. 2018). At present, active targeting and passive targeting are the major strategies for targeted tumor treatment. The delivery systems mainly include liposomes (Allen and Cullis 2013), lipid nanoparticles (Assaraf et al. 2019), albumin nanoparticles, dendrimers (Assaraf et al. 2019), gold nanoparticles (Lei et al. 2021), mesoporous silica nanoparticles, etc. (Chen et al. 2021). Before their use, nanoparticles should be evaluated for their safety (An and Zhang 2017). In nano-drug delivery systems, the main factors to be considered include (1) drug intake and release, (2) formulation stability, (3) drug safety, (4) biological distribution and targeting, etc. (Allen and Cullis 2013). It is estimated that about 20% of NPs are rejected during clinical trials due to safety concerns. Most of the nanoparticles approved or currently undergoing clinical trials include albumin and lipid-based nanoparticles (Chatterjee et al. 2017). For example, a liposomal formulation of daunorubicin (VYXEOS, CPX-351 cytarabine) is used to treat leukemia, and liposomal doxorubicin (Doxil, Caelyx) is used to treat various cancers (ovarian, breast, prostate cancer, metastatic cancer or liver cancer), nab-paclitaxel is used to treat advanced NSCLC, etc. (An and Zhang 2017). Therefore, the selection of safe drug-carrying materials is the primary concern for the clinical application of nanoparticles.

HSA is currently one of the relatively safe materials that are widely used in the treatment of clinical diseases, such as spontaneous bacterial peritonitis with ascites, refractory ascites unresponsive to diuretics, large-volume paracentesis, post-puncture syndrome symptoms, and as an adjuvant vasoconstrictor in the treatment of hepatorenal syndrome (Rozga et al. 2013; Decuzzi et al. 2021). In addition, HSA is also a multifunctional protein-carrier biomaterial (Maltas et al. 2016). Due to its hydrophobic binding pocket, HSA is used for delivering endogenous and exogenous compounds. HSA can also bind and deliver hydrophobic drugs (Chatterjee et al. 2017; Pilati and Howard 2020). HSA is a component of human blood and a nonimmunogenic endogenous protein. Albumin-based nanoparticles possess a certain level of biocompatibility (Lei et al. 2021) and are excellent nanomedicines in solid form. An example includes HSA as a lyoprotectant, which allows the dried nanoparticles to be resuspended immediately in the injection solvent to use for multifunctional bioimaging and drug delivery (An and Zhang 2017). Methotrexate–albumin conjugates, nab-bound prodrugs of doxorubicin, and nab-bound paclitaxel nanoparticles

have been clinically evaluated (Kratz 2008). Abraxane has been approved for treating metastatic breast cancer, NSCLC, and advanced (metastatic) pancreatic cancer (Hama et al. 2021). The mechanism of action of HSA in drug delivery involves interaction with the cell surface receptor gp60 (Sleep 2015). Generally, the methods for preparing albumin particles can be classified into desolvation (Arcocha-Torres et al. 2020; Langer et al. 2003), emulsification (Crisante et al. 2009), thermal gelation (Yu et al. 2006), nano-spray drying (Lee et al. 2011), and microfluidic self-assembly techniques (Tan and Ho 2018; Elzoghby et al. 2012). Studies have shown that MF-NPs-CTX prepared by microfluidic self-assembly has higher biosafety and biocompatibility than CTX-Tween (Sun et al. 2020). Albumin nanoparticles inhibit the growth of bladder tumor cells (Wang et al. 2021) by releasing doxorubicin in a controlled manner (Yang et al. 2020). Levetiracetam albumin nanoparticles can target the brain for treating epilepsy and increase drug concentration in the brain (Wilson et al. 2020), which can also be combined with intraperitoneal administration to improve efficacy (Sande et al. 2020). Some studies reported that albumin could be loaded with cabazitaxel, and the subsequent slow release enhances the antitumor efficacy of the drug (Decuzzi et al. 2021; Zhou et al. 2016). CTX-HSA-NPs prepared by the salting out method (Qu et al. 2016) are non-cytotoxic to normal human dermal fibroblasts and do not hemolyze human erythrocytes. In contrast, folic acid-modified CTX-HSA-NPs were more efficient in treating cervical cancer. These studies suggest that albumin is an excellent carrier for the delivery of cabazitaxel and can be used to treat several tumors (Chen et al. 2021). The above cabazitaxel preparations have shown great antitumor efficacy against tumors without inducing drug resistance. Therefore, we hypothesized that cabazitaxel could exert its antitumor benefits more effectively against paclitaxel/docetaxel-resistant tumors.

However, monotherapy is typically ineffective against drug-resistant tumors. Although chemotherapy has a strong tumor-killing effect, high dosages cannot be used for an extended period and thus is limited. Nucleic acid drugs such as siRNA to the target gene may encapsulated in lipid-based preparations such as ionizable lipids. This encapsulation enables the delivery of siRNA to the target tissues and cells, where they silence target genes. The surface properties of nanoparticles are designed to facilitate endosomal escape. Therefore, this study combined traditional chemotherapy with nucleic acid drug therapy to treat drug-resistant tumors. This approach retained the strong advantage of traditional chemotherapy in killing tumor cells but reduced toxicity related to traditional chemotherapy by ensuring the drug was released gradually. TGFβ-1 has been implicated in the deployment of drug resistance of lung cancer. TGFβ-1-siRNAs were synthesized and encapsulated in LNP. This preparation targeted TGFβ-1 gene silencing.

In this study, TGFβ-1 siRNA LNP, and CTX-HSA-NPs were prepared and combined to treat paclitaxel-resistant lung cancer. The gene-targeted silencing therapy and standard chemotherapy inhibited the expression of drug resistance-related proteins. This combination is a multi-channel and multi-target therapy for treating drug-resistant tumors. Overall, our preparation is an improvement of the traditional cabazitaxel therapy and is aimed at reducing the related toxicity (Fig. 1).

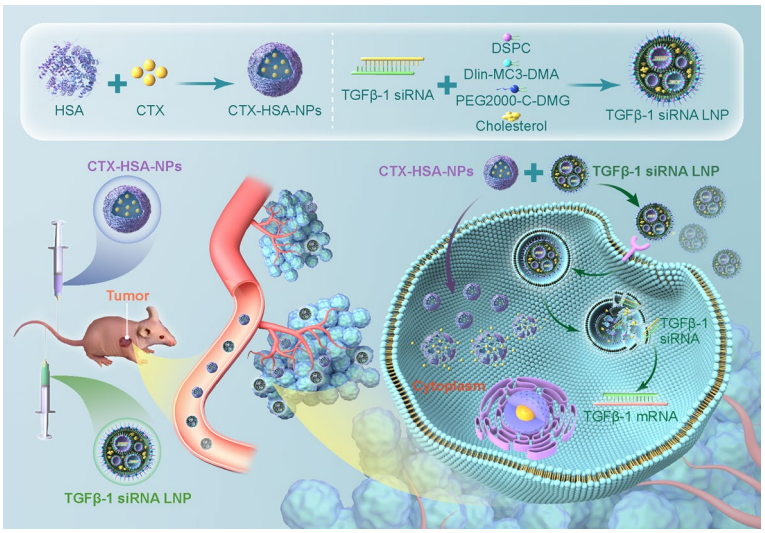

Fig. 1 CTX-HSA-NPs combined with TGFβ-1 siRNA LNP for the treatment of paclitaxel-resistant NSCLC. Cabazitaxel is a taxane antineoplastic agent that promotes the assembly of microtubule doublets into microtubules by binding to tubulin, while at the same time stabilizing microtubules by preventing their disassembly through the depolymerization process, thereby affecting mitotic and interphase cell function and inhibiting cancer cell proliferation. CTX-HSA-NPs were prepared by HSA loading of cabazitaxel. TGFβ-1 siRNA LNP were prepared by microfluidic mixing of siRNA with 4 lipids (1,2-Dioctadecanoyl-sn-glycero-3-phophocholine (DSPC), (6Z,9Z,28Z,31Z)-heptatriacont-6,9,28,31-tetraene-19-yl 4-(dimethylamino) butanoate (DLin-MC3-DMA), 1,2-dimyristoyl-rac-glycero-3-carbonylaminomethyl-ω-methoxypolyethylene glycol-2000 (PEG2000-c-DMG) and cholesterol). Combination of CTX-HSA-NPs and TGFβ-1 siRNA LNP in the treatment of paclitaxel-resistant NSCLC. TGFβ-1 siRNA LNP enters the cytoplasm and releases TGFβ-1 siRNA, which acts on the target TGFβ-1 mRNA and prevents the mRNA from being translated into protein. The expression level of TGFβ-1 is reduced and the growth of A549/T cells is inhibited. CTX-HSA-NPs is released from HSA after entering cells to kill A549/T cells

Materials and methods

Materials

Intermittent shearing machine T25 easy clean was purchased from IKA Instrument Equipment Co., Ltd (Staufen, Germany). The freeze dryer SCIENTZ-12ND was purchased from Ningbo SCIENTZ Freeze Drying Equipment Co., Ltd (Ningbo, China). Centrifuge 22331 Hamburg was purchased from Eppendorf (Germany). Homogenizer AHNANO was purchased from ATS Industrial Systems Co., Ltd (Canada). The low-temperature cooling circulation pump DLSK-3/15 was purchased from Zhengzhou Ketai laboratory equipment Co., Ltd (Zhengzhou, China). Rotary evaporator RE-201D was purchased from Hangzhou David Science and Education Instrument Co., Ltd (Hangzhou, China). The nanometer particle size potentiometer Nicomp Z3000 was purchased from PSS particle sizer company (USA). TEM transmission electron microscope Tecnai 12 was purchased from Philips company (Holland). High-performance liquid chromatography (1260 Infinity II) was purchased from Agilent Technologies (USA). PFP column 4.6 × 300 mm, 5 μm was purchased from Welch Technology Co., Ltd (Shanghai, China). The cell culture incubator FORMA STERI-CYCLE i160 was purchased from Thermo (USA). INano L rapid nano-drug preparation system and microfluidic chip SHM were purchased from Micro & Nano Company (Shanghai, China). Ultrafiltration centrifuge tubes (macrosep, 100kD) were purchased from

Pall Corporation (USA). Spark microplate reader was purchased from Tecan (Switzerland). The low-temperature high-speed centrifuge Micro17R was purchased from Thermo (USA). Electrophoresis instrument (1703930), electrophoresis tank (1703930), and membrane transfer instrument (1,703,930) were purchased from BIO-RAD (USA).

Cabazitaxel was purchased from Sichuan Xieli Pharmaceutical Co., Ltd (Sichuan, China). Human Albumin (10 g, 20%, 50 ml/bottle) was purchased from Baxter (Vienna, Austria). TGFβ-1 siRNA: sense (5′-3′): aacgaaaucuaugacaaguuc, antisense (5′-3′): acuugucauagauuucguugu was purchased from Shanghai Sangon Biotech (Shanghai, China). DSPC, DLin-MC3-DMA, PEG2000-c-DMG and cholesterol were purchased from Shanghai AVT Pharmaceutical Technology Co., Ltd (Shanghai, China). RiboGreen was purchased from Thermo (USA). Emulsifier OP was purchased from Sinopharm Chemical Reagent Co., Ltd. 1 × Tris–EDTA buffer was purchased from Beijing leaguene Biotech Co., Ltd (Beijing, China). RNase-free water was purchased from Shanghai DingGuo Biotech Co., Ltd (Shanghai, China). 0.5 M DTT, protease inhibitors, PBST (10×) were purchased from Beyotime Biotechnology (Shanghai, China). BCA protein quantification kit and 180KDa protein marker were purchased from Vazyme Biotechnology Co., Ltd (Nanjing, China). 30% acylamide was purchased from Shanghai Sangon Biotech (Shanghai, China). 1.5 M Tris pH 8.8, 1.0 M Tris PH6.8, 10% sodium dodecyl sulfate (SDS) were purchased from Coolaber (Beijing, China). Polyvinylidene difluoride (PVDF) membranes were purchased from Millipore (USA). TEMED was purchased from Aladdin (Shanghai, China). Special-grade fetal bovine serum, penicillin–streptomycin solution, and RPMI-1640 medium were purchased from Exell Biotechnology Co., Ltd (Shanghai, China). Trypsin cell digestion solution and ammonium persulfate were purchased from Genview (USA). Cell Counting Kit-8 (CCK-8) was purchased from Meilunbio (Dalian, China). Cell-grade dimethylsulfoxide (DMSO) was purchased from Solarbio Life Sciences (Beijing, China).

Cell lines and laboratory animals

Human-derived NSCLC cell line A549 and the paclitaxel-resistant NSCLC cell line A549/T were purchased from Jiangsu KeyGEN Biotechnology Co., Ltd (Nanjing, China) and identified by Suzhou Genetic Testing Biotechnology Co., Ltd (Suzhou, China). A549 and A549/T cell lines were cultured at 37 °C under 5% CO_2 in RPMI-1640 culture media supplemented with 1% penicillin–streptomycin solution (PS), and 10% fetal bovine serum (FBS).

BALB/c nude mice for the efficacy experiment were purchased from Shanghai Lingchang Biotechnology Co., Ltd (Shanghai, China). SPF grade ICR mice for acute toxicity experiments were purchased from Shanghai SLAC Laboratory Animal Co., Ltd (Shanghai, China).

CTX-HSA-NPs

Preparation of CTX-HSA-NPs HSA was dissolved in water as the aqueous phase, and cabazitaxel was dissolved in an organic solvent containing chloroform and ethanol (chloroform/ethanol = 9/1) as the organic phase. CTX-HSA-NPs was prepared through the following 4 steps: ① the organic phase was injected into the aqueous phase and then

sheared at high speed to form colostrum; ② the colostrum was homogenized for 4 min at a pressure of 1500 bar by rapid cycling-cooling homogenization method; ③ the organic solvent was removed by desolvation method to obtain the CTX-HSA-NPs. ④ The CTX-HSA-NPs were filtered with a 0.22-μm sterile filter. After determining their concentrations by HPLC, the filtered CTX-HSA-NPs were added to vials and lyophilized to obtain a white powder. Three kinds of nanoparticles, CTX-HSA-NPs (6:1), CTX-HSA-NPs (8:1), and CTX-HSA-NPs (10:1), were prepared by adjusting the ratio of HSA/CTX. The three HSA/CTX ratios of CTX-HSA-NPs were used to study the delivery and in vivo efficacy of CTX.

To prepare CTX-Tween, 2.4 g of CTX was added to 31.2 ml of absolute ethanol, and the mixture was dissolved completely by ultrasonication. Thereafter, 62.4 g of Tween-80 was added, and the solution was completely mixed by stirring at 300 rpm. The mixture was then dispensed into sterile cillin bottles.

Characterization of CTX-HSA-NPs The particle size and Polydispersity Index (PDI) of CTX-HSA-NPs were determined by dynamic light scattering method (DLS, PSS Nicomp 380 Z3000 Zeta Potential and Nano particle Size meter, PSS, USA). For zeta-potential detection, the CTX-HSA-NPs was dissolved in water and diluted with a buffer (pH 7.4). The size and morphology of CTX-HSA-NPs were detected by transmission electron microscopy (TEM) and scanning electron microscopy (SEM).

Content detecting method of CTX-HSA-NPs High-performance liquid chromatography (HPLC) was used to establish a method for detecting CTX-HSA-NPs. The mobile phase was sonicated ultrapure water containing 55% acetonitrile and 0.02% formic acid. The HPLC detection conditions were as follows: injection volume of 20 μl, UV detection wavelength of 230 nm, reference wavelength of (400 ± 100) nm, a flow rate of 1 ml/min, column temperature of 24 °C, detection time of 35 min (Agilent HPLC 1260 Infinity II, California, USA). And chromatographic column used PFP column (4.6×300 mm, 5 μm) (Welch, Shanghai, China) containing PFP short pre-column (4.6×10 mm) (Welch, Shanghai, China).

The specificity and system applicability of the method for detecting the content of CTX in CTX-HSA-NPs: The samples (A: blank solvent isopropanol, B: Free-HSA-NPs, C: CTX reference solution, D: CTX-HSA-NPs, E: CTX reference solution + CTX-HSA-NPs) were injected and detected. The chromatogram was recorded, the specificity was examined, and the number of theoretical plates and the degree of separation were calculated. The CTX reference solution and isopropanol were sampled for detection, and a standard curve was established to evaluate drug residues.

Drug entrapment efficiency (EE) and drug loading (DL) of CTX-HSA-NPs The encapsulation efficiency (EE) of CTX-HSA-NPs was detected by 0.45-μm microfiltration. The lower layer of the microfiltration membrane was CTX-encapsulated, and the upper layer of the microfiltration membrane was free-CTX. CTX-HSA-NPs were filtered using a 0.45 μm microfiltration membrane, and then the total CTX and free-CTX content was determined by HPLC, and the encapsulation efficiency (EE) and total recovery of CTX-HSA-NPs was determined using the following formulae:

$$EE = (\text{CTX-encapsulated})/(\text{free-CTX} + \text{CTX-encapsulated}) \times 100\%,$$

$$\text{Total recovery} = (\text{Free-CTX} + \text{CTX-encapsulated})/(\text{total-CTX}) \times 100\%.$$

The drug loading (DL) of CTX-HSA-NPs (6:1), CTX-HSA-NPs (8:1) and CTX-HSA-NPs (10:1) were tested by HPLC. CTX-HSA-NPs lyophilized powder in a bottle was poured out, and the empty bottle was weighed. The weight of the empty bottle was recorded as W_0. The lyophilized powder of the CTX-HSA-NPs was then dissolved in water, and the CTX content (W_1) in the bottle was determined by HPLC. The DL of CTX-HSA-NPs was determined using the following formula:

$$DL = W_1/W_0 \times 100\%.$$

The release rate of CTX-HSA-NPs CTX-HSA-NPs (6:1), CTX-HSA-NPs (8:1), and CTX-HSA-NPs (10:1) (3 mg/vial) were dissolved in 5 ml of water. The solutions were placed in a dialysis bag, clamped, and immersed in 100 ml of dialysate (1% polysorbate 80 and 2.5% ethanol in water). The CTX-HSA-NPs were mixed by magnetic stirring at 37 °C, 300 r/min. Thereafter, 1 ml of samples was taken at 0, 0.5, 1, 2, 4, 6, 8, 10, 24, and 30 h to detect the CTX-HSA-NPs content by HPLC ($n=3$). Data were processed, and a corresponding curve was drawn using the DD Solver software. The release profiles of the three CTX-HSA-NPs were analyzed and compared by Chow and Ki's Method.

Stability of CTX-HSA-NPs CTX-HSA-NPs were dissolved in normal saline, and the particle size was detected at 0 h, 2 h, 4 h, 8 h, and 24 h ($n=3$). The changes in the main parameters of particle size and size distribution within 24 h were observed. CTX-HSA-NPs were dissolved in normal saline, and the particle sizes at days 1, 2, 8, 15, 24, and 30 were determined. Changes in the particle size and distribution over 30 days were observed.

TGFβ-1 siRNA LNP

Preparation of TGFβ-1 siRNA LNP TGFβ-1 siRNA LNP was prepared using a microfluidic chip rapid nanofabrication system. The aqueous phase of acetic acid–sodium acetate buffer containing nucleic acid (siRNA) was mixed with the organic phase of ethanol solution containing 4 lipids (phospholipids, cholesterol, DLin-MC3-DMA and PEG2000-c-DMG). Phospholipids are part of the phospholipid bilayer structure of nanoparticles and mediate endosomal escape (Kanasty et al. 2013; Zuhorn et al. 2005). Cholesterol enhances LNP stability and promotes LNP fusion with biofilms (Allen and Cullis 2013; Lu et al. 2009). At endosomal pH, the ionizable lipid DLin-MC3-DMA is positively charged, facilitating cytosolic delivery and nucleic acid loading (Maier et al. 2013; Semple et al. 2010). The polyethylene glycol lipid PEG2000-c-DMG was used to prevent aggregation and increase the circulation time of the nanoparticles (Maier et al. 2013). DSPC was used as the phospholipid. DLin-MC3-DMA, DSPC, cholesterol and PEG2000-c-DMG were prepared in an appropriate ethanol solution at a molar ratio of 50:10:38.5:1.5. The TGFβ-1 siRNA was dissolved in acetic acid–sodium acetate buffer. The microfluidic chip for the

rapid nano-drug preparation system contained an organic phase and water, prepared at a ratio of 1:3. The total flow rate is 12 ml/min. Following ultrafiltration and centrifugation, the rapid nano-drug preparation system was diluted with water to a volume of 4 ml, filtered using a 0.22 μm filter.

Characterization of TGFβ-1 siRNA LNP The particle size and PDI of TGFβ-1 siRNA LNP were determined by dynamic light scattering method (DLS, PSS Nicomp 380 Z3000 Zeta Potential and Nano particle Size meter, PSS, USA). For zeta-potential detection, the TGFβ-1 siRNA LNP was dissolved in pH 6.0 and pH 7.4 buffers. The size and morphology of TGFβ-1 siRNA LNP were detected by TEM.

RiboGreen method for the content detection of TGFβ-1 siRNA Briefly, 0, 20, 50, 100, 200, 300, and 400 μl of the 2 μg/ml TGFβ-1siRNA solution were pipetted into separated tubes before adding 40 μl of 0.5% emulsifier OP. Thereafter, 960, 940, 910, 860, 760, 660, and 560 μl of 1 × TE buffer was then added, followed by 1 ml of RiboGreen diluent (diluted 200 times), to a final volume of 2 ml. The final TGFβ-1 siRNA solution concentrations were 0, 20, 50, 100, 200, 300, and 400 ng/ml. The relative fluorescence intensity was determined using a microplate reader, the excitation wavelength was 480 nm, and the emission wavelength was 530 nm. The standard curve regression equation was then calculated.

Content determination: TGFβ-1 siRNA depolymerization solution was prepared by adding 0.8 ml of 0.5% emulsifier OP to 0.1 ml of TGFβ-1 siRNA LNP. The solution was sonicated for 1 min before adding TE buffer to 10 ml of the solution. Meanwhile, 0.5 ml of 1 × TE buffer and 1 ml of RiboGreen diluent (diluted 200 times) were added to 0.5 ml of TGFβ-1 siRNA depolymerization solution. The solution was mixed well, and the fluorescence intensity was measured. The content of siRNA in the vector was calculated using the standard curve equation.

Drug entrapment efficiency (EE) of TGFβ-1 siRNA LNP Briefly, 0.3 ml of RNase-free water was added to 0.1 ml of TGFβ-1 siRNA LNP, mixed, and centrifuged at 2000×*g* for 30 min in a 300-KDa ultrafiltration centrifuge tube. The upper layer of the tube was washed with 8 ml of 1 × TE buffer, 0.8 ml of 0.5% emulsifier OP was then added, and the mixture was sonicated for 10 min. Thereafter, 1 × TE buffer was added to 10 ml of the solution and mixed well by shaking before adding 0.5 ml of 1 × TE buffer and 1 ml of RiboGreen dilution (diluted 200 times) to 0.5 ml of the mixture. The fluorescence intensity was measured, and the concentration of encapsulated siRNA and total siRNA was calculated with reference to the standard curve equation. The EE of TGFβ-1 siRNA LNP was determined using the following formula:

$EE = C_{encapsulated}/C_{total} \times 100\%$. ($C_{encapsulated}$ was the concentration of encapsulated siRNA, C_{total} was the concentration of encapsulated siRNA.)

Cytotoxicity assay

Cytotoxicity assay of CTX-HSA-NPs The paclitaxel drug resistance index (RI) of A549/T cells was detected by the CCK-8 method, and the IC_{50} of cabazitaxel API and CTX-HSA-NPs was detected on A549/T cells. A549/T cells in the logarithmic growth phase were digested with trypsin for 2 min and centrifuged at 800 rpm for 5 min. The cell pellet was

resuspended in 1–2 ml of RPMI-1640 complete medium. The cells (100 μl) were then seeded in a 96-well culture plate ($n=5$) at a density of 100 Å and incubated at 37 °C for 24 h under 5% CO_2. The culture medium was discarded after cell adherence. Drug-containing culture medium (100 μl) was added to each well, and the cells were cultured at 37 °C for 48 h under 5% CO_2. 100 μl of CCK-8 solution (10%) was added to each well before incubation at 37 °C for 2 h in the dark. The absorbance was detected at 480 nm with a microplate reader. The cell viability and RI were calculated according to the following formulas:

Cell viability $= T_{OD}/C_{OD} \times 100\%$ (T_{OD} was the average optical density (OD) of the treatment group, and C_{OD} was the average OD of the control group.)

$$RI = IC50_{A549/T}/IC50_{A549}.$$

Statistical analysis was performed using GraphPad Prism software V.8.0.2

Cytotoxicity assay of CTX-HSA-NPs combined with TGFβ-1 siRNA LNP The inhibition rate of A549/T cells was detected using CCK-8 method. The experiment was divided into four groups: ① TGFβ-1 siRNA LNP, ② CTX-HSA-NPs, ③ CTX-HSA-NPs + TGFβ-1 siRNA LNP, and ④ NC siRNA LNP. The molar ratio of TGFβ-1 siRNA LNP to CTX-HSA-NPs was fixed at 20:1, and the following concentrations were set: TGFβ-1 siRNA LNP solutions with concentrations of 0.42, 0.85, 1.69, 3.39, and 6.77 μg/ml and CTX-HSA-NPs solutions with concentrations of 1.25, 2.5, 5, 10, and 20 ng/ml were used for the assay. The molar ratio of NC siRNA LNP and CTX-HSA-NPs was fixed as 18:1, and the concentration of NC siRNA LNP was set as the control group at 0.37, 0.74, 1.49, 2.98, 5.95 μg/ml. The cells in the logarithmic growth phase were digested with trypsin, and a cell suspension of 3.5×10^4 cells/ml was prepared. Then, 100 μl of cell suspension was added to each well of a 96-well cell culture plate and incubated at 37 °C and 5% CO_2 for 24 h. After the cells adhered, the original culture medium was discarded and 100 μl of medium containing NC siRNA LNP, TGFβ-1 siRNA LNP, CTX-HSA-NPs, and CTX-HSA-NPs + TGFβ-1 siRNA LNP was added to each well. The cells were then incubated a 37 °C and 5% CO_2 for 72 h. The CCK-8 method was used to detect and calculate the inhibition rate as follows:

$$\begin{aligned}\text{Inhibition rate (\%)} = &\big(\text{OD value of negative control group}\\ &-\text{OD value of experimental group}\big)\\ &/\text{OD value of negative control group} \times 100\%.\end{aligned}$$

RT-qPCR detection of TGFβ-1 siRNA interference efficiency

A549/T cells (1.2×10^6 cells) were seeded in 6 cm cell culture dishes and incubated at 37 °C and 5% CO_2 for 24 h and then cultured in fresh drug-containing medium. A549/T cells were co-incubated with 2 μg/ml NC siRNA LNP, 2 μg/ml TGFβ-1 siRNA LNP, 4 μg/ml NC siRNA LNP and 4 μg/ml TGFβ-1 siRNA LNP for 72 h. Total RNA was extracted from A549/T cells using Cell/Tissue Total RNA Isolation Kit V_2 (KC112, Vazyme, Nanjing, China). About 1 μg of RNA was reverse transcribed into cDNA using HiScript® III All-in-one RT SuperMix Perfect for qPCR kit (R333-01, Nanjing, China). Use Taq Pro

Table 1 Primer sequences

Gene	Forward primer	Reverse primer
Human-TGFβ-1	CTAATGGTGGAAACCCACAACG	TATCGCCAGGAATTGTTGCTG
Human-β-Actin	GGGAAATCGTGCGTGACATTAAG	TGTGTTGGCGTACAGGTCTTTG

Universal SYBR qPCR Master Mix kit (Q712, Nanjing, China) for qRT-PCR detection. The sequence information of primers used in qRT-PCR is shown in Table 1. The expression level of each gene was normalized to the expression level of β-actin. Three replicates were performed for each sample.

GraphPad Prism software V.8.0.2 was used for data analysis and t test was used to analyze differences between groups.

Western blot detection of TGFβ-1 protein expression

A549/T cells (1.2×10^6 cells) were seeded in 6 cm cell culture dishes and incubated at 37 °C and 5% CO_2 for 24 h and then cultured in fresh drug-containing medium. A549/T cells were co-incubated with 4 μg/ml NC siRNA LNP or 4 μg/ml TGFβ-1 siRNA LNP for 72 h. Treated cells were lysed, and the concentration of protein in samples was detected. Subsequently, 20 μg of protein was separated on 12% sodium dodecyl sulfate–polyacrylamide gel electrophoresis and then transferred onto PVDF membrane. After 1 h of blocking using 5% non-fat dry milk at 25 ℃, the membranes were exposed to TGFβ-1 Antibody (Ab92486; Abcam, Cambridge, USA) and Anti-glyceraldehyde-3-phosphate dehydrogenase (GAPDH) antibody (5174S, CST, Danvers, Massachusetts, USA) at dilution of 1:500 and 1:1000, respectively, for 12 h at 4 ℃. The membranes were then exposed to Anti-rabbit IgG (HRP-linked Antibody) (7074P2, CST, Danvers, Massachusetts, USA) and Anti-mouse IgG (HRP-linked Antibody) (7076P2, CST, Danvers, Massachusetts, USA) both at dilution of 1:5000 for 1 h at 25 ℃. Protein bands were visualized using NcmECL Ultra ultra-sensitive chemiluminescence kit (P10200B, New cell & Molecular, Suzhou, China), and scanned using Chemiluminescence instrument ChemiScope 6200 (Clinx, Shanghai, China). ImageJ was applied to analyze the densities of protein bands.

GraphPad Prism software V.8.0.2 was used for data analysis and t test was used to analyze differences between groups.

Animal efficacy studies in vivo

In vivo efficacy study of TGFβ-1 siRNA LNP Twenty-eight 4-week-old female BALB/c nude mice were divided into 4 groups with 7 mice in each group. A cultured suspension of paclitaxel-resistant NSCLC A549/T cells was collected at a concentration of 5×10^7 cells/ml and inoculated at a dosage of 0.1 ml into the right axilla of each nude mouse subcutaneously. Tumor growth was monitored by measuring the tumor size of nude mice. When tumors grew to about 120 mm^3, animals were randomized into four groups (1) Control group, (2) 1 mg/kg NC siRNA LNP group, (3) 1.5 mg/kg CTX-Tween group, and (4) 1 mg/kg TGFβ-1 siRNA LNP group). Tail vein administration was performed twice a week, and the body weight (BW) and tumor volume (TV) of each animal were recorded every two days and used to calculate relative tumor volume (RTV). After 25 days of continuous administration, the nude mice were killed immediately, and the tumor mass was surgi-

cally removed and weighed. Tumor weight measurements were used to calculate TIR. RTV, BW and TIR were calculated using the following formulas:

(1) TV (tumor volume) $= 1/2 \times a \times b^2$. a is the length of the tumor, b was the width of the tumor.

(2) RTV (relative tumor volume) $= TV_t/TV_0$. TV_0 was the tumor volume measured on the day of grouping, and TV_t was the tumor volume monitored three times a week.

(3) T/C (%) $= T_{RTV}/C_{RTV} \times 100\%$. T_{RTV} was the RTV of the treatment group, and C_{RTV} was the RTV of the control group.

(4) TIR (%) $= (1 - TW_t/TW_c) \times 100\%$. TW_t was the tumor weight of the treatment group, and TW_c was the tumor weight of the control group.

All values were expressed as mean ± standard deviation (SD). Data were analyzed using SPSS version 18.0 and One-way analysis of variance (ANOVA) test was used to evaluate differences between groups.

In vivo efficacy study of CTX-HSA-NPs combined with TGFβ-1 siRNA LNP A549/T cell suspension was collected from sixty 4-week-old nude mice at a concentration of 2.0×10^7 cells and mixed with PBS and Matrigel at a ratio of 1:1. Then, 100 μl of the mixture was inoculated into each BALB/c nude mouse in the armpit, beginning when the tumor reached 180 mm^3. According to TV, subcutaneous tumor-bearing nude mice of paclitaxel-resistant NSCLC were randomly divided into 10 groups, with 5 mice in each group. Groups included: (1) control group (physiological saline), (2) 10 mg/kg paclitaxel injection group, (3) 5 mg/kg CTX-Tween, (4) 10 mg/kg CTX-Tween, (5) 5 mg/kg CTX-HSA-NPs (6:1), (6) 10 mg/kg CTX-HSA-NPs (6:1), (7) blank HSA preparation group, (8) 5 mg/kg CTX-HSA-NPs (8:1) group, (9) 5 mg/kg CTX-HSA-NPs (10:1) group, and (10) 5 mg/kg CTX-HSA-NPs (6:1) + 1 mg/kg TGFβ-1 siRNA LNP group. All tumor-bearing mice were administered six times within 24 days. BW and TV of each animal were recorded three times a week to use draw the BW change curve and the relative tumor growth curve. On the 25th day, all mice were killed to remove tumors and organs. The removed tumor mass was weighed for calculation of TIR. Tumors, heart, liver, spleen, lung, kidney, and stomach organs were fixed in 10% neutral buffered formalin, then paraffin-embedded and sectioned. The tumor tissue sections and the heart, liver, spleen, lung, kidney, and stomach tissue sections were stained with HE to analyze the size of tumor tissue necrosis and drug toxicity to organs. The expression of P-gp and TGFβ-1 in tumor tissue sections was detected using immunohistochemistry.

Tissue distribution of CTX-HSA-NPs in tumor-bearing nude mice

Six 4-week-old female BALB/c nude mice were divided into 2 groups with 3 mice in each group. Each nude mouse was subcutaneously inoculated in the right axilla with 0.1 ml of cultured human NSCLC cell A549/T cell suspension with a concentration of 5×10^7 cells/ml. The administration was initiated when the tumor reached 150–200 mm^3. Nude mice were divided into two groups: (1) Cypate-CTX-HSA-NPs and (2) Cypate-CTX-Tween with cypate fluorescence administered at a dose of 0.4 mg/kg. Tail vein injection was administered once, and at 0, 1, 2, 4, 8, and 24 h. Mice were placed in the small animal in vivo three-dimensional imaging system In vivo imaging system (IVIS)®

Spectrum (PerkinElmer, USA) to observe their fluorescence distribution. After 24 h, the mice were anesthetized and killed, and the tumor, heart, liver, spleen, lung, kidney, and stomach were harvested and placed in the small animal in vivo three-dimensional imaging system IVIS® Spectrum (PerkinElmer, USA) to observe the fluorescence distribution in the isolated organs. Excitation and emission wavelengths were 783 nm and 815 nm, respectively.

Acute toxicity test of CTX-HSA-NPs

In total, 120 female ICR mice aged 3–5 weeks weighing 18–22 g were divided into 12 groups, with 10 mice in each group. CTX-Tween was diluted with normal saline and injected into the tail vein of ICR mice ($n=10$) at doses of 51.16, 56.21, 61.76, 67.85, 74.55, and 81.91 mg/kg. The mice were observed for more than 14 days or until no death of the mice occurred. All abnormal conditions and deaths of the mice were recorded. CTX-HSA-NPs were injected into ICR mice ($n=10$) once through the tail vein at doses of 122.50, 137.03, 153.28, 171.46, 191.80 and 214.55 mg/kg. The mice were observed for abnormal weight loss for 14–28 days. All abnormal conditions and deaths of the mice were recorded. Mice that died during the observation period and the mice at the end of the experiment were dissected and their organs such as the heart, liver, spleen, lung, kidney, and stomach were fixed and preserved with 10% formalin. Histopathological examination of histological sections was performed with hematoxylin and eosin (HE) staining. The 50% Lethal Dose (LD_{50}) of the two groups was calculated using Lanzhou LD_{50} calculation software.

Statistical analysis

SPSS 18.0 software was used for analysis of in vivo efficacy data. All other experimental data were analyzed using GraphPad Prism software V.8.0.2. Data were expressed as mean ± SD. Experimental data were analyzed using two-tailed Student's t test and ANOVA were used for comparisons between two groups and among multiple groups, respectively. Statistical difference was defined as significant at $^{*}P<0.05$ and highly significant at $^{**}P<0.01$.

Results

CTX-HSA-NPs

Preparation and characterization of CTX-HSA-NPs

CTX-HSA-NPs (6:1), CTX-HSA-NPs (8:1), and CTX-HSA-NPs (10:1) are white translucent liquids, which form a white solid lyophilized powder after freeze-drying. The positive control (CTX-Tween) was a light yellow slightly viscous liquid whereas the blank control (Free-CTX-NPs) was a white translucent liquid, which was freeze-dried to form a white solid lyophilized powder (Fig. 2C). The particle size, PDI, zeta-potential and electron microscope characterization of CTX-HSA-NPs (6:1), CTX-HSA-NPs (8:1), and CTX-HSA-NPs (10:1) are shown in Fig. 2A, B and Table 2. The results indicated that three HSA/CTX ratios of CTX-HSA-NPs had small particle sizes of less than 120 nm and uniform distribution. The three HSA/CTX ratios of CTX-HSA-NPs exhibited stable zeta-potentials in buffer at pH 7.4 (Fig. 2A and Table 2). The results of transmission electron microscopy showed no difference in morphology and appearance of CTX-HSA-NPs

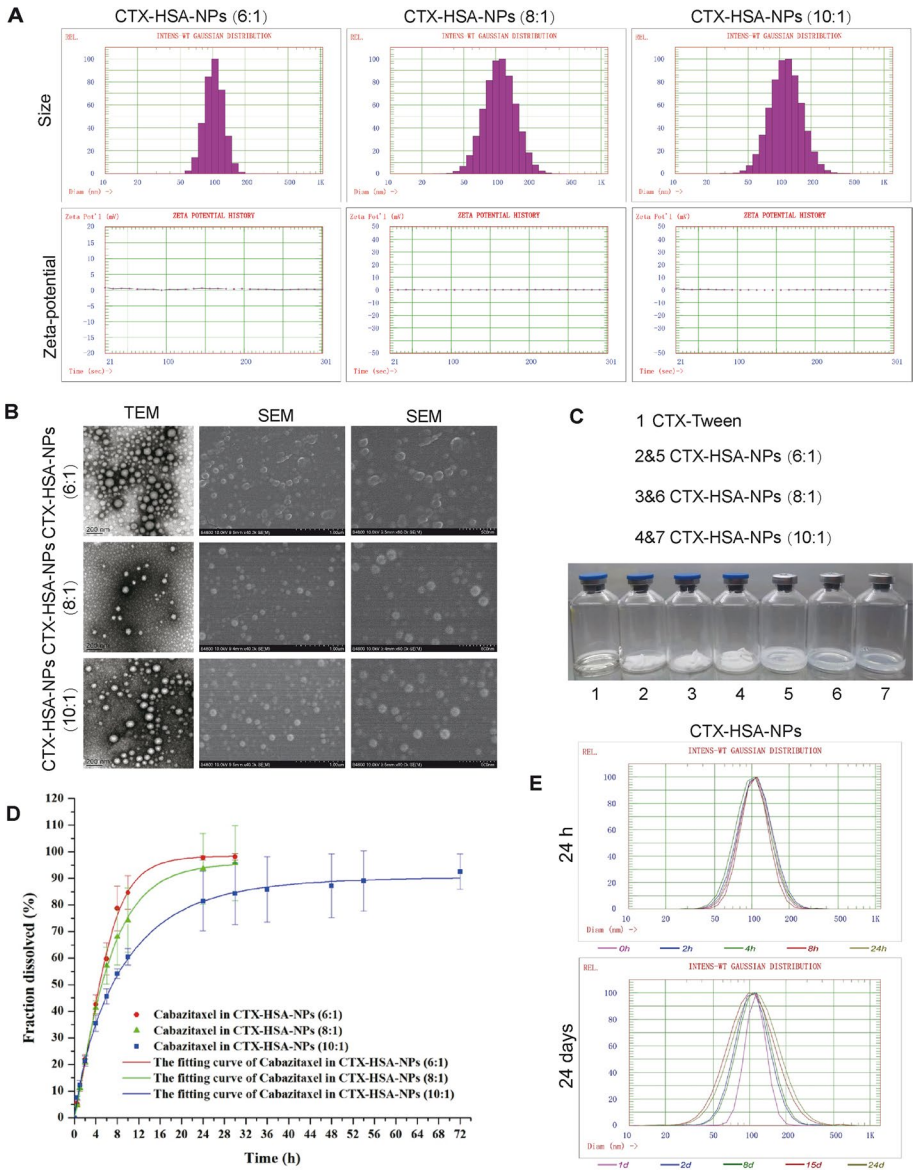

Fig. 2 Preparation and Characterization of CTX-HSA-NPs. **A** Particle sizes of CTX-HSA-NPs (6 : 1), CTX-HSA-NPs (8 : 1) and CTX-HSA-NPs (10 : 1). **B** The TEM and SEM images of CTX-HSA-NPs (6 : 1), CTX-HSA-NPs (8 : 1) and CTX-HSA-NPs (10 : 1). **C** Sample of CTX-Tween; Samples of CTX-HSA-NPs (6 : 1), CTX-HSA-NPs (8 : 1) and CTX-HSA-NPs (10 : 1) lyophilized powder (**C** 2,3,4); Sample of CTX-HSA-NPs (6 : 1), CTX-HSA-NPs (8 : 1) and CTX-HSA-NPs (10 : 1) liquid preparations (**C** 5,6,7). **D** In vitro release curves of CTX-HSA-NPs (6 : 1), CTX-HSA-NPs (8 : 1) and CTX-HSA-NPs (10 : 1). E: The stability of CTX-HSA-NPs lyophilized powder at 25 °C for 24 days after dissolving in normal saline

Table 2 Particle size and zeta-potential of CTX-HSA-NPs ($n = 3$)

Sample	Size (nm)	PDI	Zeta-potential (mV)
CTX-HSA-NPs (6 : 1)	104.50 ± 0.62	0.04 ± 0.00	0.18 ± 0.09
CTX-HSA-NPs (8 : 1)	121.87 ± 4.91	0.28 ± 0.14	0.10 ± 0.05
CTX-HSA-NPs (10 : 1)	123.37 ± 1.94	0.15 ± 0.04	0.10 ± 0.12

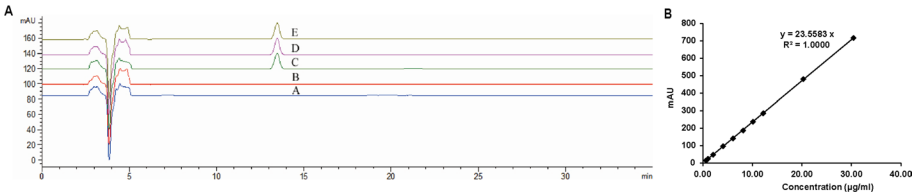

Fig. 3 Detection of CTX-HSA-NPs content. **A** The chromatogram of CTX-HSA-NPs obtained through HPLC. (Sample A is isopropanol, sample B is blank albumin nanoparticles, sample C is cabazitaxel reference solution, sample D is cabazitaxel albumin nanoparticles, E sample is cabazitaxel reference solution + cabazitaxel albumin nanoparticles). **B** The regression equation of CTX-HSA-NPs

Table 3 DL of CTX-HSA-NPs

Sample	No	W_1 (mg)	W_0 (mg)	DL (%)	Mean DL (%)
CTX-HSA-NPs (6:1)	1	41.983	355.6	11.81%	(11.96 ± 0.14)%
	2	42.182	349.0	12.09%	
	3	42.145	351.7	11.98%	
CTX-HSA-NPs (8:1)	1	2.755	35.75	7.71%	(7.22 ± 0.35)%
	2	2.469	35.11	7.03%	
	3	2.354	32.61	7.22%	
CTX-HSA-NPs (10:1)	1	2.640	47.03	5.61%	(5.57 ± 0.02)%
	2	2.473	44.37	5.57%	
	3	2.613	46.88	5.57%	

under different fields of view. In all fields of view, CTX-HSA-NPs was oval, uniformly dispersed, and similar in size, with particle sizes ranging from 50 to 100 nm (Fig. 2B). This shows that the prepared nanoparticles had smaller particle size and more uniform distribution.

Content detection of CTX in CTX-HSA-NPs

The retention time, theoretical plate, and separation degree of the CTX reference substance and CTX-HSA-NPs is about 13.4 min, greater than 8000, and greater than 1.5, respectively. The chromatogram is shown in Fig. 3. The blank solvent isopropanol and Free-HSA-NPs excipients did not interfere with the detection of CTX, as the specificity and system applicability of the CTX content detection method established by CTX-HSA-NPs were good. The standard curve results showed that the CTX reference solution was linear in the concentration range of 0.61–30.40 μg/ml. The regression equation was $y = 23.5583x$, $r = 0.99996$, and accuracy was 85–115%. After injection and analysis of high-concentration samples, the peak area of the blank solution was less than 20% of the lower limit of quantification, with no residual effect.

Drug entrapment efficiency (EE) and drug loading (DL) of CTX-HSA-NPs

The encapsulation efficiency results showed that the average encapsulation efficiency of CTX-HSA-NPs was 96.82 ± 0.20%, and average total recovery of CTX-HSA-NPs was 100.55 ± 4.19%.

Since the ratio of HSA/CTX may have some influence on the drug loading (DL), DL of CTX-HSA-NPs (6:1), CTX-HSA-NPs (8:1) and CTX-HSA-NPs (10:1) were tested in this study. The results indicated that the ratio of HSA/CTX had an effect on drug loading. Among the three HSA/CTX ratios, CTX-HSA-NPs (6:1) had the highest drug loading (Table 3). In addition, within a certain range, less HSA could load more CTX, reducing the carrier ratio, which is beneficial to increase the drug loading.

Fraction dissolved (F%) of CTX-HSA-NPs

The results of the dialysis experiments for fraction dissolved (F%) and detected release curves of CTX-HSA-NPs (6:1), CTX-HSA-NPs (8:1) and CTX-HSA-NPs (10:1) in vitro are shown in Table 4 and Fig. 2D. The results show that the release curves of CTX-HSA-NPs (6:1), CTX-HSA-NPs (8:1), and CTX-HSA-NPs (10:1) conform to the Weibull equations: $F=98.325\times\{1-\mathrm{Exp}[-((t+0.552)\text{^}1.553)/22.955]\}$, $r=0.9975$; $F=96.076\times\{1-\mathrm{Exp}[-((t-0.098)\text{^}1.077)/8.141]\}$, $r=0.9983$; and $F=90.508\times\{1-\mathrm{Exp}[-((t-0.021)\text{^}0.858)/7.430]\}$, $r=0.9951$, respectively. The results showed that CTX-HSA-NPs (6:1) was basically released within 24 h, and had a sustained release effect. CTX-HSA-NPs (8:1) was also released within 24 h but the release rate was slightly slower than that of CTX-HSA-NPs (6:1). Compared with CTX-HSA-NPs (8:1) and CTX-HSA-NPs (6:1), CTX-HSA-NPs (10:1) released CTX at the slower rate. This shows that the ratio of HSA/CTX significantly influences the release of CTX.

The release profiles of CTX-HSA-NPs (6:1), CTX-HSA-NPs (8:1), and CTX-HSA-NPs (10:1) were shown to be similar using Chow and Ki's Method Spend. Statistical analysis was carried out on the release data, and the similarity equivalence limits of the three curves were analyzed to evaluate whether the curves were similar. The results showed that the release profile of CTX-HSA-NPs (6:1) was similar to that of CTX-HSA-NPs (8:1) but dissimilar to that of CTX-HSA-NPs (10:1). The release profiles of CTX-HSA-NPs (8:1) and CTX-HSA-NPs (10:1) were not similar.

The results of release curve analysis showed that the release of CTX was slower in CTX-HSA-NPs (10:1) compared with CTX-HSA-NPs (6:1) and CTX-HSA-NPs (8:1). This result shows that the ratio of HSA/CTX has an effect on the release of nanoparticles,

Table 4 CTX-HSA-NPs Mean F%

Time (h)	CTX-HSA-NPs (6:1)	CTX-HSA-NPs (8:1)	CTX-HSA-NPs (10:1)
0	0.00% ± 0.00%	0.00% ± 0.00%	0.00% ± 0.00%
0.5	5.32% ± 1.20%	4.67% ± 0.19%	7.43% ± 0.59%
1	11.00% ± 1.05%	11.17% ± 0.83%	12.32% ± 1.54%
2	21.97% ± 1.84%	21.01% ± 1.06%	21.28% ± 1.92%
4	42.61% ± 3.54%	41.23% ± 2.74%	35.44% ± 2.98%
6	59.76% ± 6.00%	57.17% ± 6.90%	45.61% ± 2.86%
8	78.74% ± 8.41%	67.99% ± 10.64%	54.19% ± 1.82%
10	84.63% ± 6.30%	74.23% ± 12.08%	60.50% ± 3.05%
24	97.71% ± 0.86%	93.51% ± 13.36%	81.46% ± 11.14%
30	98.13% ± 1.21%	95.77% ± 14.06%	84.25% ± 11.56%

and the in vitro release of the drug is closely related to the drug's efficacy. Therefore, in a follow-up study, we investigated the effect of HSA/CTX ratio on the efficacy of CTX.

Stability of CTX-HSA-NPs

After reconstitution of CTX-HSA-NPs lyophilized powder for injection, the solution was stored at 25 ℃ for 8 h, 24 h, and 24 days. No significant change was observed in particle size and PDI, and the solution was stable at about 100 nm. These results show that the prepared CTX-HSA-NPs lyophilized powder for injection has a stable particle size within 24 days of storage at 25 ℃ after reconstitution, and has good reconstitution stability (Fig. 2E and Table 5). Thus, lyophilized powder can be efficiently reconstituted within 24 days of storage at 25 ℃ before intravenous injection without affecting the stability of the size of the nanoparticles (Table 5).

TGFβ-1 siRNA LNP

Preparation and characterization of TGFβ-1 siRNA LNP

Prepared TGFβ-1 siRNA LNP and NC siRNA LNP are clarity and transparency liquids. The average particle size of TGFβ-1 siRNA LNP was 48.1 ± 0.9 nm, with an average particle size deviation of 36.0 ± 1.2 nm, and average PDI of 0.561 ± 0.017 (Fig. 4A). The surface charge of nanoparticles is crucial for the absorption, distribution, and effect of nanoparticles (Awasthi et al. 2018). PH 6.0 buffer simulates endosome/lysosome environment with lower pH, whereas pH 7.4 buffer simulates the blood circulation environment in vivo. The mean zeta-potential of TGFβ-1 siRNA LNPs was 2.97 ± 0.23 mV in pH 6.0 buffer and − 1.47 ± 0.11 mV in pH 7.4 buffer (Fig. 4B). TGFβ-1 siRNA LNP has a weak negative charge at pH 7.4, thus it can exist more stably in the blood circulation with less side effects. In addition, it is well known that most nanoparticles enter cells through the endosome–lysosome pathway, and the endosome acidic environment is pH 4.5–7.0 (Han et al. 2020). Most nanoparticles are difficult to release into the cytoplasm after entering endosomes or lysosomes, and macromolecular drugs are easily inactivated in the presence of acidic environment and enzymes. Cytoplasmic translocation requires endosomal escape after cellular internalization which is generally achieved if the molecule of interest is either cationic or has charge reversal properties (Sun et al. 2023). This study showed that the charge of LNP reversed from negative to positive at pH 6.0,

Table 5 Stability of CTX-HSA-NPs

Time	Particle size (nm)	PDI	5% particle < (nm)	90% particle < (nm)	99% particle < (nm)
0 h	108.8 ± 0.9	0.072 ± 0.009	68.4 ± 1.8	150.5 ± 3.5	198.0 ± 7.6
2 h	111.2 ± 4.8	0.085 ± 0.012	67.2 ± 4.1	157.7 ± 7.1	212.3 ± 12.0
4 h	102.6 ± 2.7	0.038 ± 0.054	79.0 ± 16.4	126.2 ± 24.8	152.6 ± 53.4
8 h	107.7 ± 2.4	0.080 ± 0.028	66.4 ± 7.0	150.9 ± 5.3	201.4 ± 16.8
24 h	111.3 ± 2.4	0.055 ± 0.032	75.3 ± 8.7	147.3 ± 11.0	187.2 ± 26.3
48 h	111.3 ± 3.1	0.120 ± 0.054	61.5 ± 7.0	167.4 ± 18.9	238.3 ± 45.6
8 days	112.6 ± 4.6	0.125 ± 0.036	60.7 ± 4.4	171.3 ± 14.9	245.9 ± 33.5
15 days	118.0 ± 8.6	0.161 ± 0.036	58.5 ± 9.2	188.4 ± 6.8	282.3 ± 13.1
24 days	121.7 ± 0.9	0.156 ± 0.041	60.9 ± 5.8	193.5 ± 10.6	288.7 ± 30.5
30 days	221.1 ± 63.0	0.676 ± 0.197	51.4 ± 20.2	525.8 ± 138.8	1120.8 ± 307.8

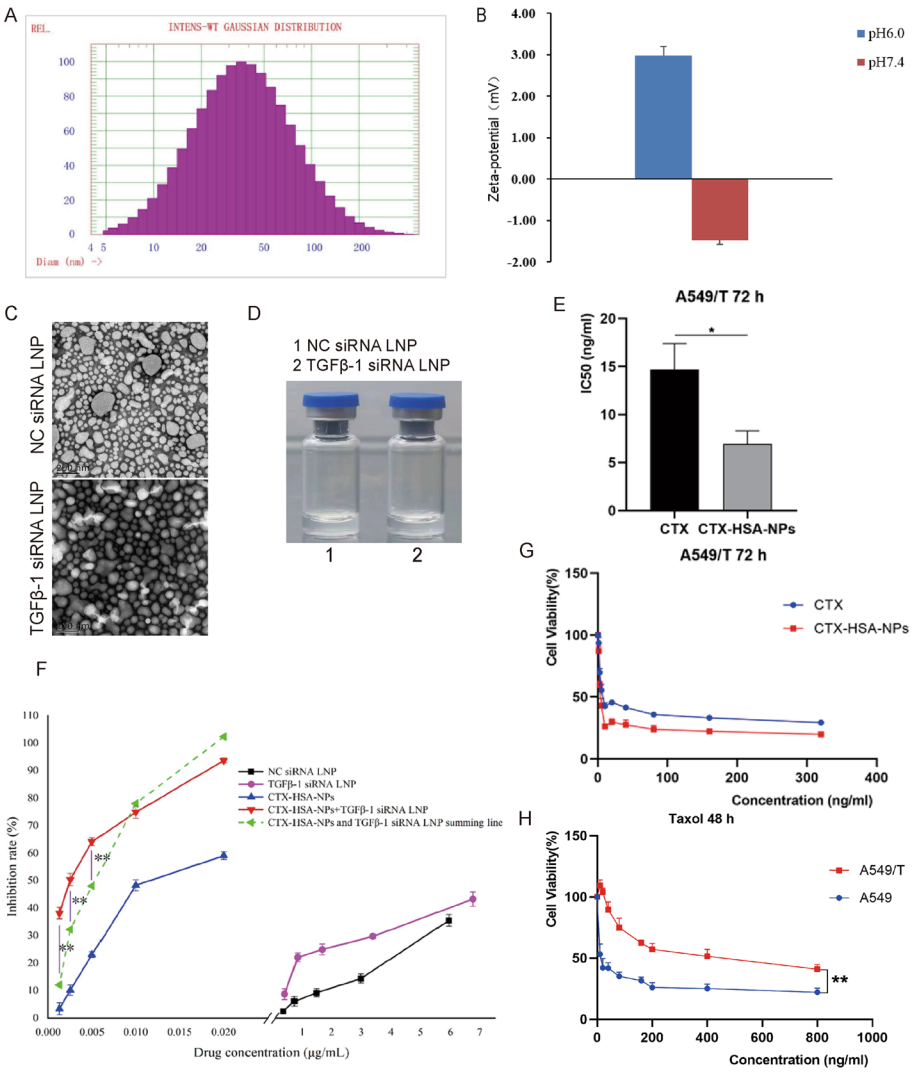

Fig. 4 Preparation and Characterization of TGFβ-1 siRNA LNP. **A** Particle size of TGFβ-1 siRNA LNP. **B** Average zeta-potential of TGFβ-1 siRNA LNP in pH 6.0 and pH 7.4 buffers. **C** TEM images of TGFβ-1 siRNA LNP. **D** Sample of NC siRNA LNP and TGFβ-1 siRNA LNP. **E** IC_{50} of cabazitaxel API and CTX-HSA-NPs on A549/T cells. **F** Combined inhibitory effect of CTX-HSA-NPs combined with TGFβ-1 siRNA LNP on A549/T cells. **G** Cytotoxicity of cabazitaxel API and CTX-HSA-NPs on A549/T cells. **H** The paclitaxel RI of A549/T cells

indicating that LNP had a charge reversal property that can cause endosomal escape. Transmission electron microscopy and scanning electron microscopy showed that most of the particles were about 50–100 nm in diameter (Fig. 4C).

Detection of TGFβ-1 siRNA LNP content

The standard curve determined by the microplate reader showed that the TGFβ-1 siRNA reference solution was linear in the range of 0 to 400 ng/ml, and the regression equation was $y = 111.68x + 357.57$, $r = 0.9999$.

Drug entrapment efficiency of TGFβ-1 siRNA LNP

Three concentrations of TGFβ-1 siRNA LNP were detected: 55.59, 57.12, and 57.86 μg/ml, averaging 56.86 ± 1.6 μg/ml. The average encapsulation efficiency of TGFβ-1 siRNA LNP samples ($n = 3$) was 97.05 ± 1.12%.

Cytotoxicity assay

Cytotoxicity assay of CTX-HSA-NPs

The IC_{50} of paclitaxel measured with CCK-8 method was 11.33 ng/ml for A549 cells and 380.6 ng/ml for A549/T cells, and the drug RI was 33.6 (Fig. 4H, $^{**}P < 0.01$). The in vitro cytotoxicity of CTX preparations detected using CCK-8 method showed that the IC_{50} of CTX crude drug and CTX-HSA-NPs on A549/T cells was 17.74 ng/ml and 5.442 ng/ml, respectively (Fig. 4G). The IC_{50} of cabazitaxel API on A549/T cells was 12.67, 13.73, and 17.74 ng/ml, averaging 14.71 ± 2.67 ng/ml. The IC_{50} of CTX-HSA-NPs on A549/T cells were 8.16, 7.159, and 5.44 ng/ml, averaging 6.92 ± 1.38 ng/ml (Fig. 4E). The IC_{50} of CTX-HSA-NPs on A549/T cells was significantly lower than that of CTX API ($^{*}P < 0.05$). The results showed that at the cellular level, CTX-HSA-NPs had a more significant inhibitory effect on the proliferation of A549/T cells than cabazitaxel API in vitro.

Cytotoxicity assay of CTX-HSA-NPs combined with TGFβ-1 siRNA LNP

The inhibition rate of CTX-HSA-NPs combined with TGFβ-1 siRNA LNP on A549/T cells was detected using CCK-8 method. The results showed that CTX-HSA-NPs and TGFβ-1 siRNA LNP and other preparations inhibited A549/T cells proliferation. The inhibitory effect of NC siRNA LNP on A549/T cells was dose-dependent, which may be due to the cation in the preparation. At medium and low concentrations, compared with NC siRNA LNP, TGFβ-1 siRNA LNP had significant higher inhibitory effect. It achieved an inhibition rate of 43.30% at a concentration of 6.77 μg/ml. Compared with CTX-HSA-NPs and TGFβ-1 siRNA LNP alone, the combined application of CTX-HSA-NPs and TGFβ-1 siRNA LNP exerted significantly higher inhibition on A549/T cells, with the inhibition rate significantly improved when combined with low and medium concentrations. This suggested that the combined drug had a synergistic effect. The cumulative value also showed a significant difference ($^{**}P < 0.01$) (Fig. 4F). Synergistic effects of the two drugs are common, such as a study in which TGFβRI inhibitor galunisertib (LY2157299) sensitized multiple B-NHL cells to doxorubicin and synergistically increased apoptosis, as well as up-regulation of p-P38 MAPK and inhibition of TGF-β/Smad2/3 and PI3K/AKT signaling pathways (Rej et al. 2023). Studies have shown that TGFβ-1 induces EMT in NSCLC (Ding et al. 2020), and TGF-β signaling pathway activity correlated positively with other cancer-relevant pathways, including EMT, breast reactive, RAS/MAPK, and RTK pathways (Korkut et al. 2018). When TGFβ-1 acts as a cancer promoting factor, it promotes the proliferation, migration and EMT of tumor cells by activating other signaling pathways, signaling molecules or microRNAs, such as the NF-κB signaling pathway and miR-133b (Skeen et al. 2013; Wang et al. 2021). Cabazitaxel is known to inhibit cancer cell proliferation by stabilizing microtubules and then affecting cell cycle mitosis (Villanueva et al. 2011). In addition, cabazitaxel has been shown to inhibit the proliferation, promote apoptosis and radiosensitivity of

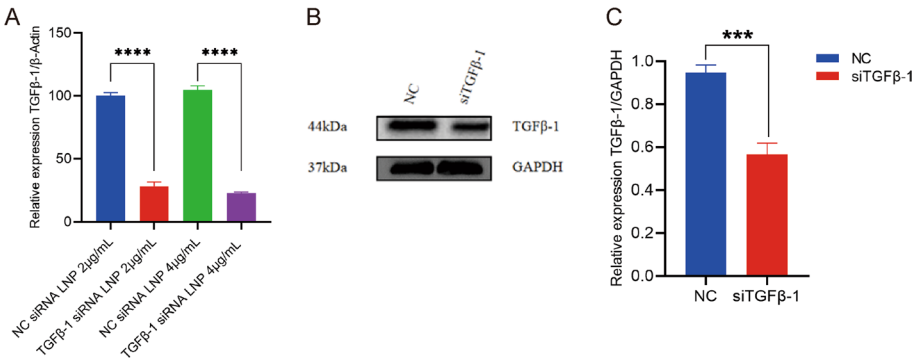

Fig. 5 RT-qPCR and Western blot detection results. **A** TGFβ-1 siRNA LNP silencing of the *TGFβ-1* gene in A549/T cells. **B** Protein bands of TGFβ-1 protein expression in A549/T cells. **C** TGFβ-1 siRNA LNP reduced the TGFβ-1 protein expression in A549/T cells. ($n = 3$)

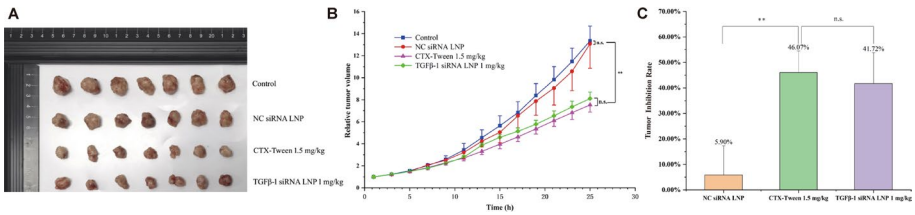

Fig. 6 In vivo efficacy of TGFβ-1 siRNA LNP. **A** Tumor tissue after TGFβ-1 siRNA LNP treatment. **B** Relative tumor growth volume of TGFβ-1 siRNA LNP and CTX-Tween. **C** TIR of TGFβ-1 siRNA LNP and CTX-Tween. ($n = 7$)

castration-resistant prostate cancer cells by inhibiting the PI3K/AKT pathway (Rej et al. 2023; Xu et al. 2022). In this study, cabazitaxel and TGFβ-1 siRNA LNP were found to have a synergistic inhibitory effect on cytotoxicity. We speculate that these two drugs exert the inhibitory effect on cell proliferation simultaneously through multiple targets of different mechanisms, and the best therapeutic effect is achieved by preventing cell mitosis as well as inhibiting TGFβ1-mediated EMT and proliferation. Through the different pathways and mechanisms mentioned above, they exert a network synergistic pharmacological effect, thereby enhancing the tumor inhibitory effect.

RT-qPCR detection of TGFβ-1 siRNA interference efficiency

The results of RT-qPCR showed that at the doses of 2 μg/ml and 4 μg/ml, compared with the NC group, the expression level of *TGFβ-1* gene in A549/T cells was significantly lower after TGFβ-1 siRNA LNP administration ($^{***}P < 0.0001$) (Fig. 5A). This demonstrated that TGFβ-1 siRNA LNP could effectively silence the *TGFβ-1* gene in A549/T cells in vitro.

Western blot detection of TGFβ-1 protein expression

Western blot results showed that compared with the NC group, the expression level of TGFβ-1 protein in A549/T cells was significantly lower after TGFβ-1 siRNA LNP

administration in vitro ($^{***}P < 0.001$) (Fig. 5B and C). This demonstrated that TGFβ-1 siRNA LNP could down-regulate TGFβ-1 protein in A549/T cells.

Animal efficacy studies in vivo

In vivo efficacy study of TGFβ-1 siRNA LNP

In vivo efficacy experiments of TGFβ-1 siRNA LNP showed that compared with NC siRNA LNP and the control group, both TGFβ-1 siRNA LNP and CTX-Tween significantly inhibited tumor growth ($^{**}P < 0.01$). There was no significant difference between NC siRNA LNP and the control group (ns, $P > 0.05$). The TIR of TGFβ-1 siRNA LNP was not significantly different from that of CTX-Tween group (ns, $P > 0.05$). The results showed that siRNA LNP preparation alone had no effect on the efficacy, and 1 mg/kg TGFβ-1 siRNA LNP showed similar efficacy as 1.5 mg/kg CTX-Tween (Fig. 6A–C).

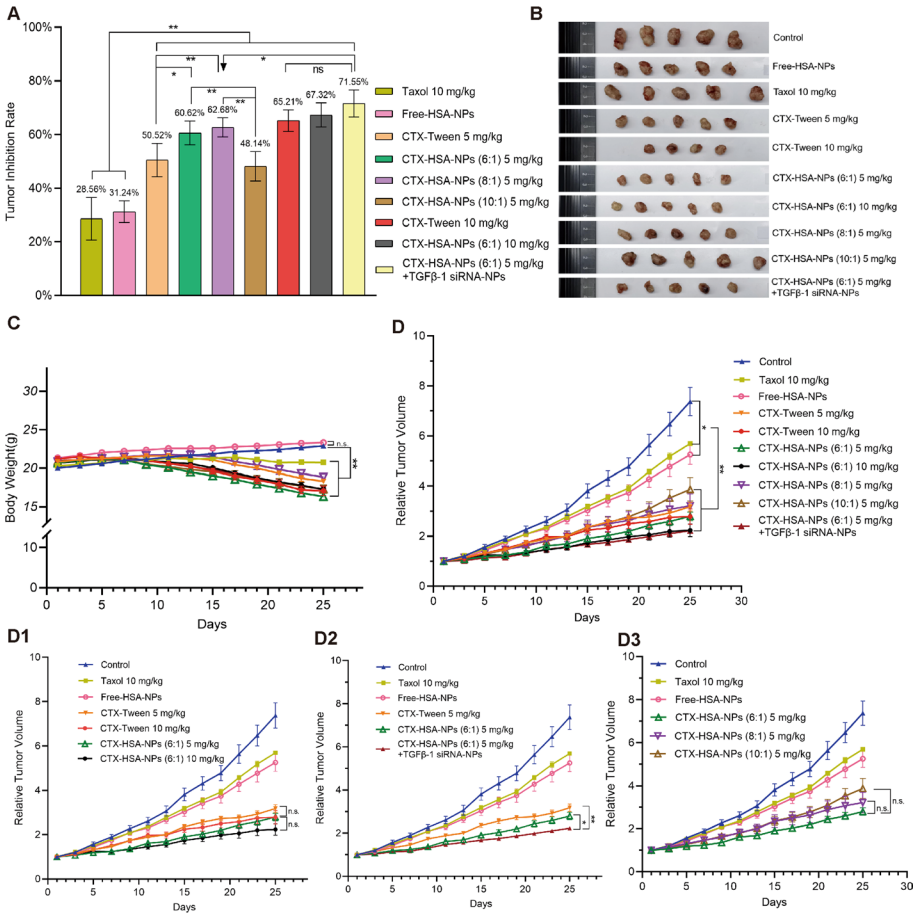

Fig. 7 In vivo efficacy of CTX-HSA-NPs combined with TGFβ-1 siRNA LNP. **A** TIR after CTX preparation and TGFβ-1 siRNA LNP treatment. **B** Tumor tissue treated with CTX preparation and TGFβ-1 siRNA LNP. **C** Growth curve of mice treated with prepared CTX and TGFβ-1 siRNA LNP. **D** RTV after treatment with CTX and TGFβ-1 siRNA LNP ($n = 5$). (To improve the clarity of RTV, the **D** are divided into **D1**, **D2** and **D3**). **D1** RTV of CTX-HSA-NPs and CTX-Tween at doses of 5 mg/kg and 10 mg/kg. **D2** The RTV of TGFβ-1 siRNA LNP and CTX-HSA-NPs combined group and CTX-HSA-NPs and CTX-Tween single group. **D3** RTV of CTX-HSA-NPs with different HSA/CTX ratios. (ns, $P > 0.05$, $^{*}P < 0.05$, $^{**}P < 0.01$) ($n = 5$)

In vivo efficacy study of CTX-HSA-NPs combined with TGFβ-1 siRNA LNP

Tumor growth of in vivo efficacy study Tumor-bearing mice in all groups were administered six doses until day 24 of the study. All mice were killed on the 25th day, and tumor tissues were removed. Removed tumors in all groups of tumor-bearing mice are shown in Fig. 7B. RTV results showed that compared with the control group, the 10 mg/kg paclitaxel group inhibited tumor growth ($^{*}P<0.05$), but its efficacy was poor, indicating that the nude mouse model was resistant to paclitaxel (Fig. 7D). TIR results showed that each administration group of CTX had significant tumor inhibition effect ($^{**}P<0.01$) (Fig. 7A). Detailed TIR analysis results are presented in Additional file 1: Table S1. In addition, compared with 5 mg/kg CTX-Tween, the TIR of the combined application group of 5 mg/kg CTX-HSA-NPs (6:1) + 1 mg/kg TGFβ-1 siRNA LNP was 21% higher ($^{**}p<0.01$) (Fig. 7A). These results show that the combined effect of the two drugs is significant. In addition, at a dose of 5 mg/kg, compared with CTX-Tween, the TIR of CTX-HSA-NPs (6:1) and CTX-HSA-NPs (8:1) was higher ($^{**}P<0.01$), indicating that at both concentration ratios, CTX-HSA-NPs was more effective than CTX-Tween (Fig. 7A). At the dose of 5 mg/kg, the efficacy of CTX-HSA-NPs (6:1) and CTX-HSA-NPs (8:1) was significantly higher than that of CTX-HSA-NPs (10:1) ($^{**}P<0.01$) (Fig. 7A). Among the three HSA/CTX ratios, CTX-HSA-NPs (8:1) had the highest antitumor efficacy.

The RTV results showed that CTX-HSA-NPs + TGFβ-1 siRNA LNP combination group had a stronger inhibitory effect on tumor growth than 5 mg/kg CTX-HSA-NPs (6:1) group ($^{*}P<0.05$), and 5 mg/kg CTX-Tween group ($^{**}P<0.01$) (Fig. 7D3). However, there was no significant difference between the 5 mg/kg and 10 mg/kg dose groups of CTX-Tween and CTX-HSA-NPs (6:1) (ns, $P>0.05$) (Fig. 7D1). Further, the three HSA/CTX ratios of CTX-HSA-NPs showed no significant difference in RTV (Fig. 7D2), indicating that the combination of CTX-HSA-NPs and TGFβ-1 siRNA LNP can enhance the antitumor efficacy of paclitaxel-resistant NSCLC mouse model, which showed some resistance to cabazitaxel.

The results of the growth and BW change curve of tumor-bearing mice showed that compared with the control group, the BW of the paclitaxel group and the CTX preparation group was lower ($^{**}P<0.01$), whereas the BW of free-HSA-NPs was close to that of the control group (ns, $P>0.05$) (Fig. 7C). HSA showed no obvious toxicity as a drug-carrying material. In the CTX preparation group, the CTX-HSA-NPs (8:1) group mice lost less weight, indicating that the ratio of HSA/CTX (8:1) was a good curative and safer ratio (Fig. 7C).

In conclusion, according to TIR results, compared with traditional CTX-Tween, CTX-HSA-NPs (8:1) had the best curative effect at the same dosage, and the curative effect was dependent on HSA/CTX ratio in CTX-HSA-NPs. The efficacy of 5 mg/kg CTX-HSA-NPs (6:1) combined with 1 mg/kg TGFβ-1 siRNA LNP was significantly higher than that of CTX-Tween or CTX-HSA-NPs alone.

H&E staining results of in vivo efficacy study The pathological section of the tumor after treatment is shown in Fig. 8. Pathological analysis revealed the following results. In the control group, no inflammatory cell infiltration and hemorrhage were found in the tumor tissue, and there was no new blood vessel in the interstitium. There were 1/3 necrotic areas in the tumors of Taxol 10 mg/kg group and Free-HSA-NPs group. The

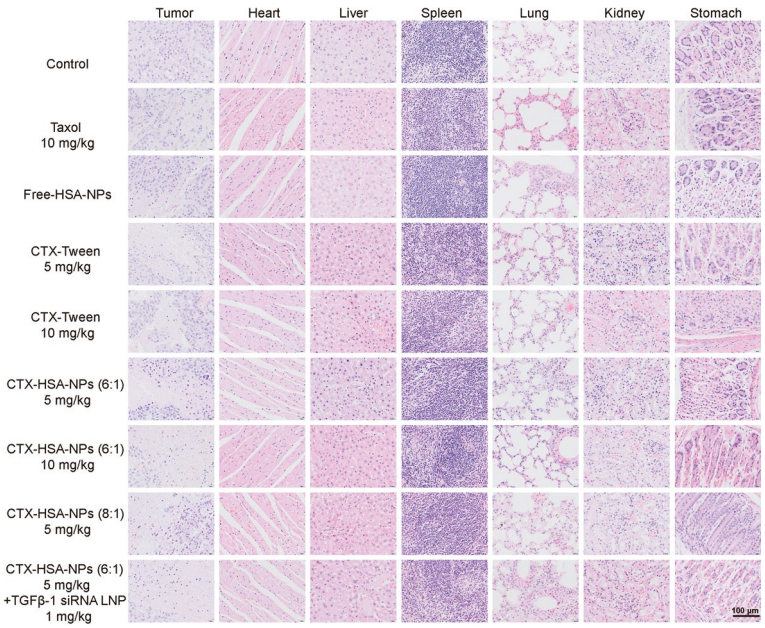

Fig. 8 Pathological sections of tumors and organs from nude mice after treatment

CTX-Tween administration groups, CTX-HSA-NPs administration groups and CTX-HSA-NPs + TGFβ-1 siRNA LNP combined administration group all had obvious apoptotic cells, central necrosis, and inflammatory cell infiltration. At a dose of 5 mg/kg, the necrotic area of CTX-Tween accounted for 1/2–2/3 of the total area, and the necrotic area of CTX-HSA-NPs (6:1) 5 mg/kg group was greater than 2/3 of the total area, the area of necrosis in the CTX-HSA-NPs (6:1) 5 mg/kg + TGFβ-1 siRNA LNP 1 mg/kg group was greater than 3/4 of the total area. It can be concluded that the area of tumor necrosis in the CTX-HSA-NPs (6:1) administration group was larger than that of CTX-Tween, and the tumor necrosis area of CTX-HSA-NPs (6:1) combined with TGFβ-1 siRNA LNP administration group was larger than that of CTX-Tween or CTX-HSA-NPs (6:1) administration group at a dose of 5 mg/kg.

The results of pathological analysis of heart, liver, spleen, lung, kidney, and stomach organs showed that all the drugs had no obvious damage to the spleen. In the paclitaxel administration group, the heart, liver, lung, kidney, and stomach all had degeneration, congestion, and inflammatory cell infiltration. Compared with the paclitaxel administration group, the degeneration, congestion and inflammatory cell infiltration in the CTX-HSA-NPs (6:1) group and the CTX-HSA-NPs (6:1) combined with TGFβ-1 siRNA LNP administration group were alleviated.

Immunohistochemistry of in vivo efficacy study Because paclitaxel-resistant non-small cell lung cancer has developed drug resistance, and P-gp is related to drug resistance, in order to compare the expression levels of P-gp in tumor tissues after treatment in different drug groups, the expression of P-gp in all groups was detected by immunohistochemistry. The main mechanism of TGFβ-1 siRNA LNP administration group to inhibit tumor growth is to silence TGFβ-1 and reduce the expression of TGFβ-1 protein. In order to compare the difference between the combination therapy and the two preparations of

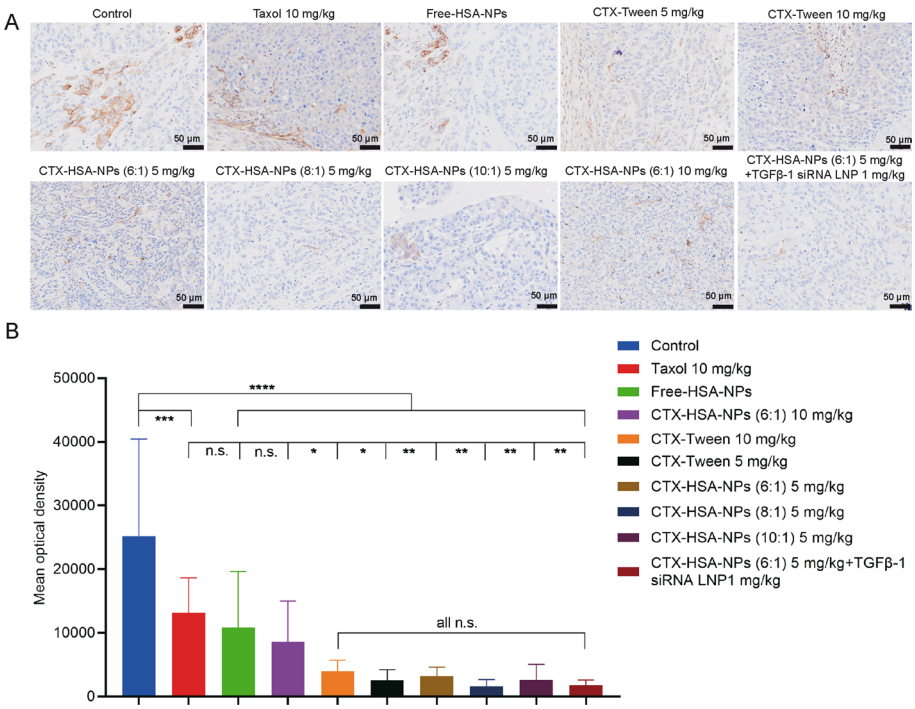

Fig. 9 Immunohistochemistry for P-gp expression in tumor tissues. **A** P-gp expression level in nude mice bearing paclitaxel-resistant non-small cell lung cancer after treatment. **B** The average optical density values of tumor immunohistochemical sections from nude mice bearing paclitaxel-resistant non-small cell lung cancer after treatment. (ns, $P > 0.05$, $^{*}P < 0.05$, $^{**}P < 0.01$) (scale bar = 50 μm) ($n = 4$)

CTX alone, the TGFβ-1 protein expression of the tumor slices of the CTX-Tween, CTX-HSA-NPs and CTX-HSA-NPs combined with TGFβ-1 siRNA LNP administration group was detected by immunohistochemistry.

The expression profile of P-gp in the tumor tissue from each treatment group is shown in Fig. 9. Compared with the control group, the expression level of P-gp in tumor tissues was significantly lower after treatment with paclitaxel and CTX preparations ($^{*}P < 0.05$). Compared with the paclitaxel treatment group, the expression levels of P-gp in the 10 mg/kg and 5 mg/kg CTX-Tween treatment groups were lower ($^{*}P < 0.05$). In addition, the expression levels of P-gp in 5 mg/kg CTX-HSA-NPs (6:1), CTX-HSA-NPs (8:1), CTX-HSA-NPs (10:1) and CTX-HSA-NPs (6:1) combined with TGFβ-1 siRNA LNP treatment group was significantly lower than that of the paclitaxel treatment group ($^{**}P < 0.01$). These results indicated that the expression of P-gp decreased after treatment with CTX-HSA-NPs or combined with TGFβ-1 siRNA LNP. Because CTX has low affinity with P-gp, it is less likely to be resistant. However, it is worth noting that the P-gp expression level after injection with 10 mg/kg CTX-HSA-NPs (6:1) was higher than that of 5 mg/kg CTX-HSA-NPs, which suggested that a high-dose treatment could promote resistance. Similarly, paclitaxel-resistant NSCLC tended to be resistant to CTX after high-dose CTX treatment. Therefore, CTX at a dose of 5 mg/kg combined with nucleic acid drugs is an effective strategy to avoid multidrug resistance in the treatment of paclitaxel-resistant NSCLC.

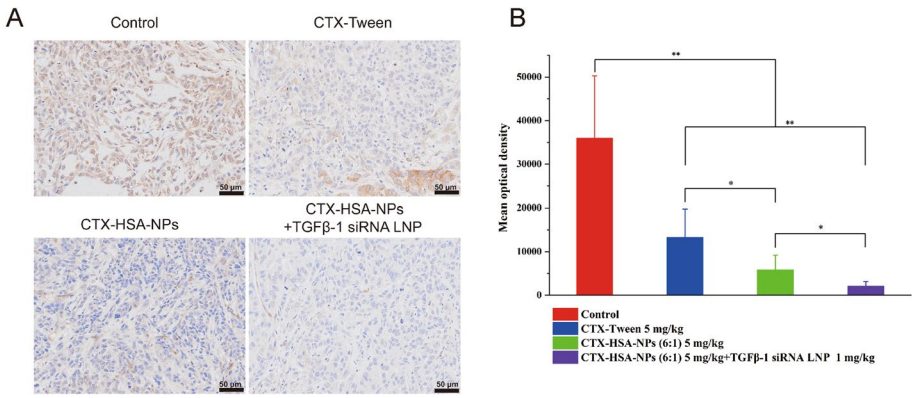

Fig. 10 TGFβ-1 siRNA LNP combined with CTX-HSA-NPs downregulated TGFβ-1 protein expression in tumor tissues. **A** TGFβ-1 expression level in nude mice bearing paclitaxel-resistant non-small cell lung cancer after treatment. **B** The average optical density values of tumor immunohistochemical sections from nude mice bearing paclitaxel-resistant non-small cell lung cancer after treatment. ($^{*}P<0.05$, $^{**}P<0.01$) (scale bar = 50 μm) ($n=4$)

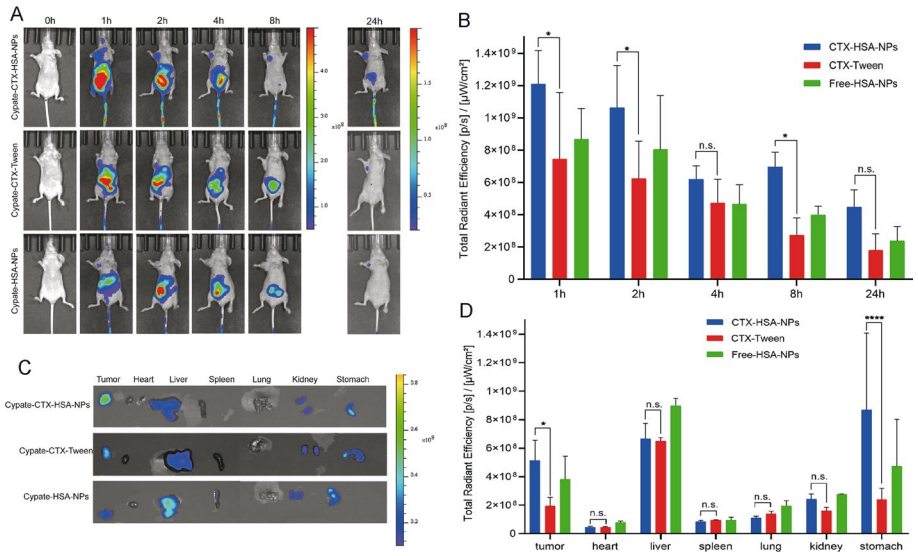

Fig. 11 Cypate-CTX-HSA-NPs was distributed in more tissues compared with Cypate-CTX-Tween at different time-points. **A** Bioluminescence signal distribution in paclitaxel-resistant tumor. **B** Quantitative analysis of paclitaxel-resistant tumor bioluminescence signals at different time-points. **C** Ex vivo bioluminescence images of tissues from the tumor, liver, heart, spleen, lung, and kidney at 24 h post-injection. **D** Quantitative analysis of bioluminescence signals of tissues from the tumor, liver, heart, spleen, lung, and kidney at 24 h post-injection. $C_{Cypate} = 0.4$ mg/kg

The results of TGFβ-1 expression in tumor tissues of each treatment group are shown in Fig. 10. The average optical density value of the control group, 5 mg/kg CTX-Tween treatment group, 5 mg/kg CTX-HSA-NPs (6:1) treatment group, CTX-HSA-NPs (6:1) + TGFβ-1 siRNA LNP combined treatment group was 35,995.8 ± 14,272.0, 13,250.3 ± 6527.3, 5866.1 ± 3324.3, and 2065.5 ± 1131.9, respectively. There were significant differences among the four groups (one-way ANOVA analysis, $F=42.849$, $^{***}P<0.001$). Compared with the control group, after 5 mg/kg CTX-Tween, 5 mg/kg CTX-HSA-NPs (6:1) and CTX-HSA-NPs (6:1) + TGFβ-1 siRNA LNP treatment, the

Table 6 LD_{50} of CTX-Tween

Groups	Doses (mg/kg)	*n*	Dead animals	Mortality (%)
1	51.16	10	0	0
2	56.21	10	0	0
3	61.76	10	4	40
4	67.85	10	4	40
5	74.55	10	7	70
6	81.91	10	8	80

Regression equation: $y = -13.0899 + 9.8838x$ ($r = 0.9439$)

Table 7 LD_{50} of CTX-HSA-NPs

Groups	Doses (mg/kg)	*n*	Dead animals	Mortality (%)
7	122.50	10	0	0
8	137.03	10	0	0
9	153.28	10	1	10
10	171.46	10	2	20
11	191.8	10	5	50
12	214.55	10	8	80

Regression equation: $y = -28.7235 + 14.7901x$ ($r = 0.9909$)

expression level of TGFβ-1 was significantly lower (Dunnett T3 method for pairwise comparison, $^{**}P < 0.01$). The results indicated TGFβ-1 was up-regulated after the tumor tissue became resistant to paclitaxel in the tumor-bearing nude mouse model. CTX-Tween group, CTX-HSA-NPs group, and TGFβ-1 siRNA LNP combined with CTX-HSA-NPs group could down-regulate TGFβ-1 protein. The decrease in the expression level of TGFβ-1 in the combined treatment group was higher than that in CTX-HSA-NPs ($^{*}P < 0.05$). In addition, CTX-HSA-NPs caused a higher decrease in the expression level of TGFβ-1 than CTX-Tween ($^{*}P < 0.05$). Compared with CTX-HSA-NPs alone, the combination therapy showed greater ability to inhibit the expression of TGFβ-1.

Tissue distribution of CTX-HSA-NPs in tumor-bearing nude mice

The tumor tissue distribution of Cypate-CTX-HSA-NPs was higher than that of Cypate-CTX-Tween. The tissue distribution in tumor-bearing nude mice was detected at 1–24 h post-injection, and the fluorescence intensity of Cypate-CTX-HSA-NPs in tumors at 1 h, 2 h, and 8 h was higher than that of Cypate-CTX-Tween ($^{*}P < 0.05$) (Fig. 11A, B). The drug was mainly distributed in the tumor, liver and stomach tissues after 24 h, and the fluorescence intensity of Cypate-CTX-HSA-NPs in the tumor was higher than that of Cypate-CTX-Tween ($^{*}P < 0.05$) (Fig. 11C, D). There was no significant difference in the distribution of the drugs in the heart, liver, spleen, lung and kidney, and the distribution of Cypate-CTX-HSA-NPs in the stomach was significantly higher than that of Cypate-CTX-Tween ($^{****}P < 0.0001$) (Fig. 11C, D).

Acute toxicity test of CTX-HSA-NPs

The results of acute toxicity experiments showed that compared with CTX-Tween, the LD_{50} of CTX-HSA-NPs was 2.82 times higher but its toxicity was 1.8 times lower. After

14 days post-injection observation, a total of 22 and 12 mice died in the CTX-Tween group at a dose of 51.16–81.91 mg/kg and the CTX-HSA-NPs group at a dose of 122.50–214.55 mg/kg, respectively. Compared with CTX-Tween, CTX-HSA-NPs were less toxic and improved survival time and survival rate at 14 days post-injection. On the 14th day of the post-injection observation period, some mice in the two groups still continued to lose weight and showed significantly lower activity levels. Therefore, the observation period was extended to 28th day post-injection until the mice did not experience weight loss and malaise. The observation was ended when they returned to normal vital signs and activities. During the 28 days of post-injection observation, a total of 23 mice died in the CTX-Tween group at a dose of 51.16–81.91 mg/kg compared with 16 mice that died in the CTX-HSA-NPs group at a dose of 122.50–214.55 mg/kg. These results indicated that the toxicity of CTX-HSA-NPs at 14 days or 28 days post-injection was significantly lower than that of CTX-Tween, and CTX-HSA-NPs improved survival time and survival rate (Tables 6, 7).

The results of organ pathological section analysis showed similar histopathological changes in the CTX-Tween group and the CTX-HSA-NPs group after one administration, with reduced damage to the organs in the CTX-HSA-NPs group. In CTX-Tween group, myocardial cells were slightly atrophied, spleen was severely atrophied, lymphocytes were significantly reduced or even disappeared, alveolar walls were moderately thickened, interstitial inflammatory cells infiltration and hemorrhage, and renal tubules were mildly degenerated and necrotic. In the CTX-HSA-NPs group, the structure of the heart was normal, the spleen was moderately atrophied, the lymphocytes were moderately reduced, the alveolar wall was slightly thickened, and the kidney histology was normal. Compared with the 67.85 mg/kg CTX-Tween group, the 191.80 mg/kg CTX-HSA-NPs group had less damage to organs, including significantly less lung damage, and slightly less damage to the heart, liver, kidney and spleen (Fig. 12).

Discussion

The multidrug resistance of lung cancer has always been an urgent problem to be solved in clinical practice, and achieving targeted and low toxicity is an area of interest in cancer treatment. Possible mechanisms of MDR in chemotherapy include enhanced drug efflux (Tan et al. 2021), genetic factors (gene mutations, amplifications, and epigenetic alterations), growth factors, increased DNA repair capacity, increased anti-apoptotic

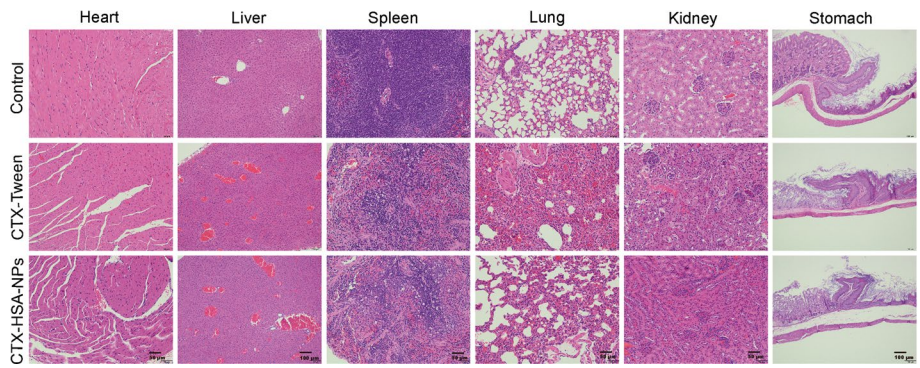

Fig. 12 HE-stained pathological sections of mouse organs

potential, and decreased permeability (Assaraf et al. 2019; Wu et al. 2014). These mechanisms are the main reason for the reduced efficacy of antitumor drug therapy.

Small interfering RNAs are small RNA fragments of specific length and sequence produced by the cleavage of double-stranded RNA expressed by foreign invading genes (Sharp 1999). RNA interference is the process by which small RNA molecules complementarily to interrupt the coding of target gene sequences by inducing degradation of the corresponding messenger RNA (mRNA) and preventing the translation of mRNA into protein (Sharp 1999). Therefore, RNA interference is selective and stimulates the silencing of its complementary target mRNA, hence potentially useful as a cancer therapy approach, which also has important implications for gene regulation and disease treatment. TGFβ-1 is involved in the regulation of multidrug resistance and can induce cellular EMT to promote lung cancer cell migration, invasion, and anti-apoptosis. Therefore, silencing TGFβ-1 by siRNA has great significance in the treatment of multidrug resistance in NSCLC.

CTX is a tubulin inhibitor (Hardin et al. 2017), which disrupts the cell cycle by inducing G2/M arrest and inhibits the growth of tumor cells by inhibiting the depolymerization of tubulin and promoting the assembly of tubulin (Muggia and Kudlowitz 2014). In addition, CTX can also promote apoptosis by inhibiting the cell cycle and blocking the mitotic pathway (Villanueva et al. 2011). Compared with docetaxel and paclitaxel, CTX is structurally methyl etherified and has a weaker P-glycoprotein affinity (Duran et al. 2018). Because of this property, CTX inhibits the growth of tumor cells that are resistant to paclitaxel and docetaxel (Paller and Antonarakis 2011). In addition, due to its low affinity for P-glycoprotein and good pharmacokinetic properties, CTX has broad application potential, and has attracted more and more research attention in recent years. Some studies have reported the therapeutic effect of CTX on drug-resistant tumors. One study found that CTX is a potentially effective drug against HCC after chemotherapy resistance caused by P-gp overexpression and acquired sorafenib resistance, and may improve the prognosis of patients with advanced HCC (Chen et al. 2018). Studies have confirmed that CTX can inhibit the proliferation of U87MG glioblastoma cells and enhance radiosensitivity. Its mechanism of action involves inhibiting the cell cycle and promoting apoptosis after ionizing radiation (Neshasteh-Riz et al. 2018). Studies have shown that CTX exerts anti-metastatic and cytotoxic effects in glioma cells by inducing apoptosis and strongly inhibiting tumor angiogenesis without affecting normal angiogenesis. It eliminates cancer cells and tumor blood vessels while preserving brain function, and protects healthy nerve tissue (Ghoochani et al. 2016). Studies have shown that CTX effectively improves chemotherapy resistance, and the co-loading of flexible composite liposomes with CTX and β-elemene significantly improved the efficacy of paclitaxel-resistant lung adenocarcinoma (Zeng et al. 2019). CTX also significantly inhibited the growth of hepatocellular carcinoma (HCC) in vivo. In the chemotherapy-resistant HCC cell Huh-TS-48 with P-gp overexpression, CTX showed low cross-resistance to other chemotherapeutic drugs, suggesting its potential for the treatment of drug-resistant liver cancer (Chen et al. 2018).

This study used a dual approach of reducing the toxicity of traditional chemotherapy drugs and targeting gene silencing to study refractory and drug-resistant tumors. TGFβ-1 siRNA LNP were prepared by mixing lipids containing phospholipids,

cholesterol, DLin-MC3-DMA and PEG2000-c-DMG with acetate–sodium acetate buffer containing TGFβ-1 siRNA using a microfluidic chip. The prepared TGFβ-1 siRNA LNP showed advantageous characteristics of small particle size and high encapsulation efficiency. TGFβ-1 siRNA LNP was weakly negatively charged in blood circulation at pH 7.4, could exist more stably in blood circulation with less side effects, and was positively charged in endosomes/lysosomes with lower pH, demonstrating its endosome escape function. RT-qPCR results showed that the expression level of *TGFβ-1* gene in A549/T cells was significantly decreased after TGFβ-1 siRNA treatment at doses of 2 μg/ml and 4 μg/ml compared with NC group ($P < 0.01$). Western blot results showed that compared with the NC group, the expression level of TGFβ-1 protein in A549/T cells was significantly lower after TGFβ-1 siRNA treatment ($P < 0.01$). In vitro results showed that TGFβ-1 siRNA LNP could effectively silence *TGFβ-1* gene and inhibit TGFβ-1 protein expression in A549/T cells. Cells take up LNPs through apolipoprotein E (ApoE)-dependent and/or ApoE-independent pathways. After acidification in endosomes, protonated LNPs induce a hexagonal phase structure and destroy the cell membrane, to release RNA molecules, which induce the degradation of TGFβ-1 mRNA, preventing its translation into TGFβ-1 protein and achieving TGFβ-1 silencing. In vivo experiments showed that TGFβ-1 siRNA LNP could effectively inhibit the growth of paclitaxel-resistant NSCLC tumors, and the immunohistochemical results of the tumors verified the down-regulation of TGFβ-1 expression.

In this study, human serum albumin was used to prepare CTX-HSA-NPs, which was lyophilized using a rapid cycling cooling homogenization method and desolvation method. The prepared CTX-HSA-NPs lyophilized powder has the advantages of small particle size, narrow particle size distribution, high encapsulation efficiency, and high stability after dissolved. In vitro, compared with CTX-HSA-NPs or TGFβ-1 siRNA LNP alone, inhibition of CTX-HSA-NPs in combination with TGFβ-1 siRNA LNP on A549/T cells was significantly higher ($^{**}P < 0.01$), demonstrating the synergistic effect of the combination. RT-qPCR showed that compared with the NC group, the TGFβ-1 siRNA LNP dose at the rate 2 μg/ml and 4 μg/ml, respectively, significantly decreased the expression level *TGFβ-1* gene in A549/T cells ($^{**}P < 0.01$). Western blot results showed that compared with the NC group, the expression level of TGFβ-1 protein in A549/T cells was significantly low in the TGFβ-1 siRNA group ($^{**}P < 0.01$). The mice in vivo results showed that the distribution of the drug in the tumor tissue was higher in the Cypate-CTX-HSA-NPs group than in the Cypate-CTX-Tween group. In vivo efficacy results showed that the tumor inhibition rates (TIR) of CTX-HSA-NPs (6:1) and (8:1) (60.62% and 62.68%) were significantly higher than those of CTX-Tween (50.52%). Compared with CTX-Tween (50.52%), the combined application of CTX-HSA-NPs and TGFβ-1 siRNA LNP (71.55%) increased the TIR by 21%, which was significantly higher.

These results indicated using the half dose of CTX combined with TGFβ-1 siRNA LNP can achieve the effect of doubling the dose of CTX. The results of tumor immunohistochemistry showed that TGFβ-1 siRNA LNP significantly inhibited the expression of TGFβ-1, and compared with other groups, the expression of P-gp after low-dose CTX-HSA-NPs treatment was lower, which did not cause obvious drug resistance. Acute toxicity results showed that the LD_{50} of CTX-Tween was 67.648 mg/kg, while that of

CTX-HSA-NPs was 190.609 mg/kg. The toxicity of CTX-HSA-NPs was 1.8 folds lower than that of CTX-Tween.

In this study, there are still some shortcomings. This study found that the combination therapy of CTX-HSA-NPs and TGFβ-1 siRNA LNP has a good anti-drug resistance effect, and the mechanism of the interaction between the two drugs still needs further research.

Conclusion

In summary, HSA nanoparticles are excellent carriers of CTX, and the preparation of CTX-HSA-NPs reduces the toxicity of traditional CTX injection preparations, effectively inhibits the growth of paclitaxel-resistant NSCLC tumors, and inhibits the expression of P-gp. TGFβ-1 is involved in the occurrence and development of paclitaxel-resistant NSCLC tumors, and the expression of TGFβ-1 increases after A549 cells become resistant to paclitaxel. After treatment with TGFβ-1 siRNA LNP and CTX-HSA-NPs, *TGFβ-1* target mRNA can be silenced to down-regulate TGFβ-1 protein expression, thereby inhibiting the growth of paclitaxel-resistant NSCLC tumors. Therefore, CTX-HSA-NPs is a potentially effective drug against paclitaxel-resistant tumors. Combining TGFβ-1 siRNA LNP and CTX-HSA-NPs in the treatment of paclitaxel-resistant lung adenocarcinoma not only achieves gene-targeted therapy but also improves the safety of chemotherapy. Combination therapy is a promising novel approach to the treatment of paclitaxel-resistant NSCLC as well as refractory and multidrug-resistant tumors.

Abbreviations

LNP	Lipid nanoparticles
CTX	Cabazitaxel
HSA	Human serum albumin
NPs	Nanoparticles
CTX-HSA-NPs	Cabazitaxel albumin nanoparticles
TGFβ-1	Transforming growth factor beta-1
siRNA	Small interfering RNA
TGFβ-1 siRNA LNP	TGFβ-1 siRNA lipid nanoparticles
NSCLC	Non-small cell lung cancer
DSPC	1,2-Dioctadecanoyl-sn-glycero-3-phophocholine
DLin-MC3-DMA	(6Z,9Z,28Z,31Z)-Heptatriacont-6,9,28,31-tetraene-19-yl 4-(dimethylamino) butanoate
PEG2000-c-DMG	1,2-Dimyristoyl-rac-glycero-3-carbonylaminomethyl-ω-methoxypolyethylene glycol-2000
TIR	Tumor inhibition rates
MDR	Multi-drug resistance
PDI	Polydispersity Index
DL	Drug loading
F%	Fraction dissolved
EE	Entrapment efficiency
HCC	Hepatocellular carcinoma
ApoE	Apolipoprotein E
DLS	Dynamic light scattering
TEM	Transmission electron microscopy
SEM	Scanning electron microscopy
HPLC	High-performance liquid chromatography
RI	Drug resistance index
OD	Optical density
TIR	Tumor inhibition rates
BW	Body weight
TV	Tumor volume
RTV	Relative tumor volume
HE	Hematoxylin and eosin
LD_{50}	50% Lethal dose
IC_{50}	Half maximal inhibitory concentration
ANOVA	Analysis of variance

SD	Standard deviation
CCK-8	Cell Counting Kit-8
FBS	Fetal bovine serum
IVIS	In vivo imaging system
SDS	Sodium dodecyl sulfate
PS	Penicillin–streptomycin solution
EMT	Epithelial–mesenchymal transition

Supplementary Information

The online version contains supplementary material available at https://doi.org/10.1186/s12645-023-00194-7.

Additional file 1: Table S1. Analysis results of TIR (Student's t test).

Author contributions

TT, ZZ and TX conceived and designed the experiment. TT, YF, and WW carried out the experiment. TT, RW, LY, analyzed data and summarized results. TT and YZ drafted the manuscript and drew the figures. TT, ZZ and TX revised the manuscript. All authors read and approved the final manuscript.

Funding

This work was supported by Program of Basic Public Welfare Research in Zhejiang Province of China (Grant No. LGF20H300006), National Natural Science Foundation of China (Grant No. 81730108), Key Project of Zhejiang project Ministry of Science and Technology (Grant No. 2021C03087), Key Project of Hangzhou Ministry of Science and Technology (Grant No. 20212013B03).

Availability of data and materials

All data generated or analyzed during this study are included in this article.

Declarations

Ethics approval and consent to participate

The protocols for the animal experiments were approved by the Scientific Research Ethics Committee of Hangzhou Normal University (HangZhou, China) (No: HSD20210701), and was conducted in accordance with the guidelines for handling laboratory animals in China (2006-398). The reference number for the animal use license is SYXK (Zhejiang) 2020-0026.

Consent for publication

We give our consent for the manuscript to be published in *Journal of Nanobiotechnology*.

Competing interests

The authors declare no conflict of interest.

Received: 14 January 2023 Accepted: 8 April 2023
Published online: 29 July 2023

References

Allen TM, Cullis PR (2013) Liposomal drug delivery systems: from concept to clinical applications. Adv Drug Deliv Rev 65(1):36–48
An FF, Zhang XH (2017) Strategies for preparing albumin-based nanoparticles for multifunctional bioimaging and drug delivery. Theranostics 7(15):3667–3689
Arnst J (2020) When Taxol met tubulin. J Biol Chem 295(41):13994–13995
Assaraf YG, Brozovic A, Gonçalves AC et al (2019) The multi-factorial nature of clinical multidrug resistance in cancer. Drug Resist Updat 46:100645
Awasthi R, Roseblade A, Hansbro PM et al (2018) Nanoparticles in cancer treatment: opportunities and obstacles. Curr Drug Targets 19(14):1696–1709
Chatterjee M, Ben-Josef E, Robb R et al (2017) Caveolae-mediated endocytosis is critical for albumin cellular uptake and response to albumin-bound chemotherapy. Cancer Res 77(21):5925–5937
Chen R, Cheng Q, Owusu-Ansah KG et al (2018) Cabazitaxel, a novel chemotherapeutic alternative for drug-resistant hepatocellular carcinoma. Am J Cancer Res 8(7):1297–1306
Chen Y, Pan Y, Hu D et al (2021) Recent progress in nanoformulations of cabazitaxel. Biomed Mater 16:032002
Crisante F, Francolini I, Bellusci M et al (2009) Antibiotic delivery polyurethanes containing albumin and polyallylamine nanoparticles. Eur J Pharm Sci 36(4–5):555–564
de Arcocha-Torres M, Quincoces G, Martínez-López AL et al (2020) Preparation, radiolabeling with (99m)Tc and (67)Ga and biodistribution studies of albumin nanoparticles covered with polymers. Rev Esp Med Nucl Imagen Mol (engl Ed) 39(4):225–232
Decuzzi P, Peer D, Mascolo DD et al (2021) Roadmap on nanomedicine. Nanotechnology 32(1):012001
Ding Z, Du W, Lei Z et al (2020) Neuropilin 1 modulates TGF-β1-induced epithelial-mesenchymal transition in non-small cell lung cancer. Int J Oncol 56(2):531–543

Duran GE, Derdau V, Weitz D et al (2018) Cabazitaxel is more active than first-generation taxanes in ABCB1(+) cell lines due to its reduced affinity for P-glycoprotein. Cancer Chemother Pharmacol 81(6):1095–1103
Elbashir SM, Harborth J, Lendeckel W et al (2001) Duplexes of 21-nucleotide RNAs mediate RNA interference in cultured mammalian cells. Nature 411(6836):494–498
Elzoghby AO, Samy WM, Elgindy NA (2012) Albumin-based nanoparticles as potential controlled release drug delivery systems. J Control Release 157(2):168–182
Ghoochani A, Hatipoglu Majernik G, Sehm T et al (2016) Cabazitaxel operates anti-metastatic and cytotoxic via apoptosis induction and stalls brain tumor angiogenesis. Oncotarget 7(25):38306–38318
Guo H, Hou Y, Ding J (2019) Nanomedicines for intravesical chemotherapy in bladder cancer. Curr Pharm Des 25(4):371–373
Hama M, Ishima Y, Chuang VTG et al (2021) Evidence for delivery of abraxane via a denatured-albumin transport system. ACS Appl Mater Interfaces 13(17):19736–19744
Han Y, Zhou J, Hu Y et al (2020) Polyphenol-based nanoparticles for intracellular protein delivery via competing supramolecular interactions. ACS Nano 14(10):12972–12981
Hardin C, Shum E, Singh AP et al (2017) Emerging treatment using tubulin inhibitors in advanced non-small cell lung cancer. Expert Opin Pharmacother 18(7):701–716
Irigoyen M, Pajares MJ, Agorreta J et al (2010) TGFBI expression is associated with a better response to chemotherapy in NSCLC. Mol Cancer 9:130
Jackson AL, Linsley PS (2010) Recognizing and avoiding siRNA off-target effects for target identification and therapeutic application. Nat Rev Drug Discov 9(1):57–67
Kanasty R, Dorkin JR, Vegas A et al (2013) Delivery materials for siRNA therapeutics. Nat Mater 12(11):967–977
Kim YJ, Choi WI, Jeon BN et al (2014) Stereospecific effects of ginsenoside 20-Rg3 inhibits TGF-β1-induced epithelial-mesenchymal transition and suppresses lung cancer migration, invasion and anoikis resistance. Toxicology 322:23–33
Korkut A, Zaidi S, Kanchi RS et al (2018) A pan-cancer analysis reveals high-frequency genetic alterations in mediators of signaling by the TGF-β superfamily. Cell Syst 7(4):422-437.e427
Kratz F (2008) Albumin as a drug carrier: design of prodrugs, drug conjugates and nanoparticles. J Control Release 132(3):171–183
Król M, Pawłowski KM, Majchrzak K et al (2010) Why chemotherapy can fail? Pol J Vet Sci 13(2):399–406
Langer K, Balthasar S, Vogel V et al (2003) Optimization of the preparation process for human serum albumin (HSA) nanoparticles. Int J Pharm 257(1–2):169–180
Lee SH, Heng D, Ng WK et al (2011) Nano spray drying: a novel method for preparing protein nanoparticles for protein therapy. Int J Pharm 403(1–2):192–200
Lei C, Liu XR, Chen QB et al (2021) Hyaluronic acid and albumin based nanoparticles for drug delivery. J Control Release 331:416–433
Liu H, Wang W, Zhang G et al (2017) Role of TGF-β1 in multi-drug resistance in small cell lung cancer and its clinical significance. Zhong Nan Da Xue Xue Bao Yi Xue Ban 42(4):419–425
Lu JJ, Langer R, Chen J (2009) A novel mechanism is involved in cationic lipid-mediated functional siRNA delivery. Mol Pharm 6(3):763–771
Maier MA, Jayaraman M, Matsuda S et al (2013) Biodegradable lipids enabling rapidly eliminated lipid nanoparticles for systemic delivery of RNAi therapeutics. Mol Ther 21(8):1570–1578
Mainini F, Eccles MR (2020) Lipid and Polymer-Based Nanoparticle siRNA Delivery Systems for Cancer Therapy. Molecules 25(11):2692
Malhotra M, Dhingra R, Sharma T et al (2013) Cabazitaxel: a novel drug for hormone-refractory prostate cancer. Mini Rev Med Chem 13(6):915–920
Maltas E, Gubbuk IH, Yildiz S (2016) Development of doxorubicin loading platform based albumin-sporopollenin as drug carrier. Biochem Biophys Rep 7:201–205
Mansoori B, Mohammadi A, Davudian S et al (2017) The different mechanisms of cancer drug resistance: a brief review. Adv Pharm Bull 7(3):339–348
Muggia F, Kudlowitz D (2014) Novel taxanes. Anticancer Drugs 25(5):593–598
Neshasteh-Riz A, Zeinizade E, Safa M et al (2018) Cabazitaxel inhibits proliferation and potentiates the radiation response of U87MG glioblastoma cells. Cell Biol Int 42(7):815–822
Paller CJ, Antonarakis ES (2011) Cabazitaxel: a novel second-line treatment for metastatic castration-resistant prostate cancer. Drug Des Devel Ther 5:117–124
Pilati D, Howard KA (2020) Albumin-based drug designs for pharmacokinetic modulation. Expert Opin Drug Metab Toxicol 16(9):783–795
Qu N, Lee RJ, Sun Y et al (2016) Cabazitaxel-loaded human serum albumin nanoparticles as a therapeutic agent against prostate cancer. Int J Nanomed 11:3451–3459
Reck M, Remon J, Hellmann MD (2022) First-line immunotherapy for non-small-cell lung cancer. J Clin Oncol 40(6):586–597
Rej A, Paladhi A, Daripa S et al (2023) Galunisertib synergistically potentiates the doxorubicin-mediated antitumor effect and kick-starts the immune system against aggressive lymphoma. Int Immunopharmacol 114:109521
Rozga J, Piątek T, Małkowski P (2013) Human albumin: old, new, and emerging applications. Ann Transpl 18:205–217
Semple SC, Akinc A, Chen J et al (2010) Rational design of cationic lipids for siRNA delivery. Nat Biotechnol 28(2):172–176
Setten RL, Rossi JJ, Han SP (2019) The current state and future directions of RNAi-based therapeutics. Nat Rev Drug Discov 18(6):421–446
Sharp PA (1999) RNAi and double-strand RNA. Genes Dev 13(2):139–141
Skeen VR, Collard TJ, Southern SL et al (2013) BAG-1 suppresses expression of the key regulatory cytokine transforming growth factor β (TGF-β1) in colorectal tumour cells. Oncogene 32(38):4490–4499
Sleep D (2015) Albumin and its application in drug delivery. Expert Opin Drug Deliv 12(5):793–812
Sun Y, Lee RJ, Meng F et al (2020) Microfluidic self-assembly of high cabazitaxel loading albumin nanoparticles. Nanoscale 12(32):16928–16933

Sun R, Zhang Y, Lin X et al (2023) Aminopeptidase N-responsive conjugates with tunable charge-reversal properties for highly efficient tumor accumulation and penetration. Angew Chem Int Ed Engl 62(9):e202217408
Sung H, Ferlay J, Siegel RL et al (2021) Global cancer statistics 2020: GLOBOCAN estimates of incidence and mortality worldwide for 36 cancers in 185 countries. CA Cancer J Clin 71(3):209–249
Suzuki Y, Ishihara H (2021) Difference in the lipid nanoparticle technology employed in three approved siRNA (Patisiran) and mRNA (COVID-19 vaccine) drugs. Drug Metab Pharmacokinet 41:100424
Tan YL, Ho HK (2018) Navigating albumin-based nanoparticles through various drug delivery routes. Drug Discov Today 23(5):1108–1114
Tan T, Li J, Luo R et al (2021) Recent advances in understanding the mechanisms of elemene in reversing drug resistance in tumor cells: a review. Molecules 26(19):5792
Van de Sande L, Cosyns S, Willaert W et al (2020) Albumin-based cancer therapeutics for intraperitoneal drug delivery: a review. Drug Deliv 27(1):40–53
Villanueva C, Bazan F, Kim S et al (2011) Cabazitaxel: a novel microtubule inhibitor. Drugs 71(10):1251–1258
Vrignaud P, Sémiond D, Lejeune P et al (2013) Preclinical antitumor activity of cabazitaxel, a semisynthetic taxane active in taxane-resistant tumors. Clin Cancer Res 19(11):2973–2983
Vrignaud P, Semiond D, Benning V et al (2014) Preclinical profile of cabazitaxel. Drug Des Devel Ther 8:1851–1867
Wang L, Tao H, Li Z et al (2021) Preparation of composite cypate nanoparticles and its application in the treatment of pediatric bladder tumors. J Nanosci Nanotechnol 21(2):868–877
Wang J, Xiang H, Lu Y et al (2021) Role and clinical significance of TGF-β1 and TGF-βR1 in malignant tumors (review). Int J Mol Med 47(4):55
Whelan J (2005) First clinical data on RNAi. Drug Discov Today 10(15):1014–1015
Wilson B, Selvam J, Mukundan GK et al (2020) Albumin nanoparticles coated with polysorbate 80 for the targeted delivery of antiepileptic drug levetiracetam into the brain. Drug Deliv Transl Res 10(6):1853–1861
Wu Q, Yang Z, Nie Y et al (2014) Multi-drug resistance in cancer chemotherapeutics: mechanisms and lab approaches. Cancer Lett 347(2):159–166
Xu Z, Xu L, Ge Y et al (2022) Cabazitaxel suppresses the proliferation and promotes the apoptosis and radiosensitivity of castration-resistant prostate cancer cells by inhibiting PI3K/AKT pathway. Am J Transl Res 14(1):166–181
Yang Z, Zhang N, Ma T et al (2020) Engineered bovine serum albumin-based nanoparticles with pH-sensitivity for doxorubicin delivery and controlled release. Drug Deliv 27(1):1156–1164
Yu S, Yao P, Jiang M et al (2006) Nanogels prepared by self-assembly of oppositely charged globular proteins. Biopolymers 83(2):148–158
Zeng YY, Zeng YJ, Zhang NN et al (2019) The preparation, determination of a flexible complex liposome co-loaded with cabazitaxel and β-elemene, and animal pharmacodynamics on paclitaxel-resistant lung adenocarcinoma. Molecules 24(9):1697
Zhang E, Xing R, Liu S et al (2019) Current advances in development of new docetaxel formulations. Expert Opin Drug Deliv 16(3):301–312
Zhou G, Jin X, Zhu P et al (2016) Human serum albumin nanoparticles as a novel delivery system for cabazitaxel. Anticancer Res 36(4):1649–1656
Zuhorn IS, Bakowsky U, Polushkin E et al (2005) Nonbilayer phase of lipoplex-membrane mixture determines endosomal escape of genetic cargo and transfection efficiency. Mol Ther 11(5):801–810

Publisher's Note